VNiVERSiDAD D SALAMANCA

Facultad de ciencias

Chaotic Phase of the Bose-Hubbard Hamiltonian in an external static field

María del Pilar Martín Clavero

Supervised by: Alberto Rodríguez González

July 2024

VNiVERSiDAD D SALAMANCA

Facultad de ciencias

Chaotic Phase of the Bose-Hubbard Hamiltonian in an external static field

María del Pilar Martín Clavero

Supervised by: Alberto Rodríguez González

July 2024

Abstract

In this thesis, we study the emergence of a chaotic phase in the tilted Bose-Hubbard Hamiltonian, consisting in a one dimensional lattice with an additional linear potential occupied by a fixed number of bosons that can interact and tunnel to next-neighbouring sites of the lattice.

In order to do this study, we make use of *Random Matrix Theory*, as well as of some basic notions about the special features of the eigenstates that can emerge on such chaotic regime. The purpose of the thesis is to characterize this chaotic phase as a function of the system parameters, namely the tunneling energy, the particle interaction strength and the amplitude of the external field that induces the lattice tilt. So as to achieve this, numerical simulations of the evolution of the system with these parameters are carried out. The simulations consist in fixing, first, the interaction to one, and then choosing a value for the external field (measured in units of the interaction). Next, we vary the tunneling energy. We calculate the eigenenergies of the system and use them to get the *level spacing ratio* associated to a short range feature of the energy spectrum. Such figure of merit is compared against Random Matrix Theory in order to prove the emergence of quantum chaos. Later, we analyze the structure of the eigenstates to show its connection with such chaos. In order to do so, we obtain the *first generalized fractal dimensions*, as well as their mean value and variance (over close-in-energy eigenstates), which we use as indicators of the degree of delocalization of the eigenstates in Hilbert space, and correlate with the presence of quantum chaos.

Similarly, we perform another set of simulations with the tunneling energy fixed to one and the interaction strength chosen in units of the tunneling energy. We study the emergence of chaos via the variation of the external field, using the same figures of merit for the energy spectrum and the eigenstates as previously.

These simulations are then used to conclude that the three parameters of the Hamiltonian must be similar in order to observe quantum chaos. Moreover, these results allow us to analyze the emergence of quantum chaos from the perspective of a particular state that is typically used in experimental dynamical studies with cold atoms, namely the state in which each site of the lattice is occupied by only one boson. One can therefore read off the range of parameters where the dynamical consequences of the chaotic phase could be observed experimentally.

Lastly, we fix all the system parameters and choose two specific *rescaled energy* values, for which we obtain the closest-in-energy eigenstates to study the evolution of the mean and variance of the *first generalized fractal dimension* with Hilbert space size, and verify its accordance with Random Matrix Theory predictions.

Keywords: Tilted Bose-Hubbard Hamiltonian, generalized fractal dimension, delocalization, quantum chaos, Fock space, avoided crossings, bosons, eigenstate structure, energy spectrum.

Resumen

En este trabajo nos dedicamos al estudio de la aparición de la fase caótica en el Hamiltoniano de Bose-Hubbard en presencia de un campo externo estático, consistente en una red unidimensional a la que se le añade un potencial lineal que es ocupada por un número fijo de bosones, capaces de interactuar entre sí y pasar de un sitio de la red a los dos adyacentes a través de efecto túnel.

Para hacer el estudio, hacemos uso de la Teoría de Matrices Aleatorias, así como de algunas nociones básicas acerca de algunas propiedades especiales que aparecen en los autoestados del sistema en el régimen caótico. Así, el propósito de este trabajo es caracterizar esta fase caótica como función de los parámetros del sistema, concretamente la energía asociada al transporte de bosones por efecto túnel, la fuerza de interacción entre partículas y la amplitud del campo externo que da lugar a la inclinación de la red. Para ello, realizamos una serie de simulaciones numéricas de la evolución del sistema con dichos parámetros. Las simulaciones consisten, en primer lugar, en fijar la energía de interacción a la unidad, para después escoger un valor (medido en unidades del parámetro de interacción) del campo externo. Después, la energía asociada al *tunneling* se va variando. Se calculan las autoenergías del sistema para posteriormente utilizarse en el cálculo del valor de la *razón entre el espaciado de niveles*, calculado para un rango corto de valores del espectro energético. Esta figura de mérito se compara con la Teoría de Matrices Aleatorias para probar la aparición de caos cuántico. También, analizamos la estructura de los autoestados para mostrar su relación con la aparición de dicho caos. Para ello, calculamos las *primeras dimensiones fractales generalizadas*, así como su valor medio y su varianza (de nuevo, sobre un conjunto de estados próximos en energía), para utilizarlas como indicadores del grado de deslocalización de los autoestados en el espacio de Hilbert, y para relacionarlas con la presencia de caos cúantico.

De manera similar, llevamos a cabo otro conjunto de simulaciones, en que el término que fijamos a la unidad es el de *tunneling*, y elegimos un valor para la fuerza de interacción en unidades de la energía de *tunneling*. Estudiamos la aparición de caos, entonces, a través de la variación del campo externo, utilizando las mismas figuras de mérito para el espectro energético y los autoestados que utilizamos anteriormente.

Los resultados de estas simulaciones se usan para concluir que los tres parámetros del Hamiltoniano han de ser comparables para poder observar el caos cuántico. Además, los resultados permiten analizar la aparición de la fase caótica desde la perspectiva de un estado particular típicamente utilizado en estudios experimentales dinámicos con átomos fríos, correspondiente al estado en que cada sitio de la red es ocupado por un único bosón. Así, uno puede leer directamente el rango de parámetros en que podrían observarse experimentalmente las implicaciones dinámicas de la fase caótica.

Finalmente, fijamos todos los parámetros del sistema y elegimos dos *energías normalizadas* concretas, para las cuales obtenemos los autoestados más próximos en energía a ellas para

estudiar la evolución del valor medio y la varianza de las *primeras dimensiones fractales generalizadas* con la dimensión del espacio de Hilbert, y verificamos su concordancia con las predicciones de la Teoría de Matrices Aleatorias.

Palabras clave: Hamiltoniano de Bose-Hubbard, dimensión fractal generalizada, deslocalización, caos cuántico, espacio de Fock, repulsión de niveles, bosones, estructura de autoestados, espectro energético.

Contents

List of Figures

List of Tables

1 | Introduction

1.1 Scientific context

Quantum simulation can provide valuable insight into difficult quantum problems in physics or chemistry. Ultracold atoms in optical lattices represent an ideal platform for simulations of quantum many-body problems that are relevant to diverse fields such as condensed matter physics, statistical physics, quantum chemistry and high-energy physics [8, 10, 11]. These ultracold atoms provide a useful tool to implement a variety of bosonic and fermionic Hamiltonians with a very precise control of the system parameters. One of such Hamiltonians is the Bose-Hubbard Hamiltonian [5, 19].

Via simulations with ultracold atoms, several macroscopic phenomena can be observed. This is the case, for example, of the phase transition that the ground state of the Bose-Hubbard Hamiltonian undergoes when the relative strength of two competing energy terms in the Hamiltonian is varied across a critical value, beyond which the system goes from a superfluid phase to a Mott insulator phase [9].

Apart from regular lattices, tilted lattices offer a useful way to observe some other interesting macroscopical properties. For example, magnetic phenomena is also studied using ultracold atoms that emulate spin Hamiltonians. In the same way superfluid and Mott insulator phases can be studied, a paramagnetic to antiferromagnetic transition can be observed by controlling the strength of the Hamiltonian interaction term, as depicted in Fig. 1.1.

Another problem that can be investigated experimentally with ultracold gases in tilted lattices are Bloch oscillations [18]. When studying the dynamics of a single-particle in a

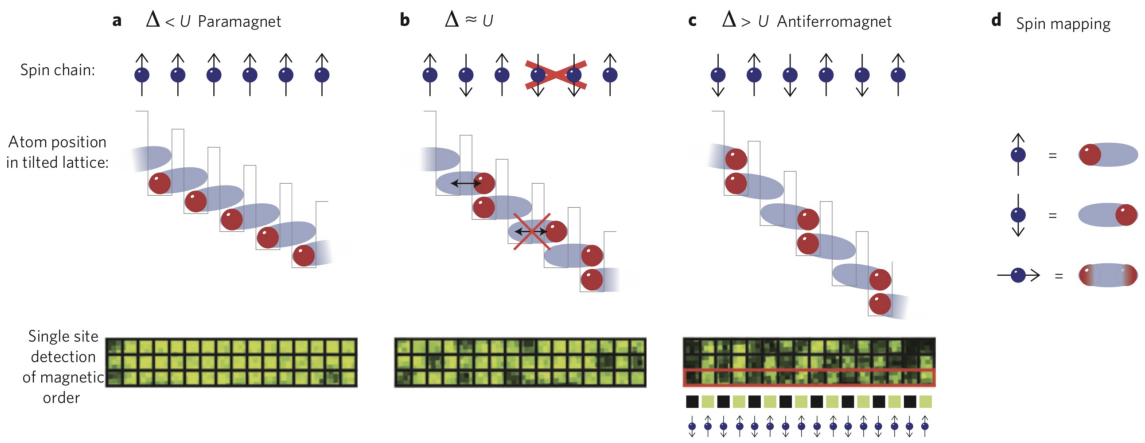

Figure 1.1: Realization of a quantum Ising model using a one-dimensional Mott insulator in a strong potential gradient. This figure has been taken from Ref. [2].

one dimensional periodic potential under the influence of a static force, one may naively expect to find a steady accelerated motion. However, the actual dynamics consist in a coherent oscillation whose period is inversely proportional to the lattice constant and to the static force [14]. It was in 1992 when the fabrication of semiconductor superlattices allowed the experimental observation of such phenomena. However, a problem occurs when making use of superlattices, as Bloch oscillations are hindered by relaxation processes [18]. Optical lattices, on their part, overcome this difficulty. Laser waves and cold neutral atoms play the role of crystal lattices and electrons, respectively, making it possible to mitigate such problems. Consequently, optical lattices have offered a unique opportunity to study Bloch oscillations [1, 6, 13].

In general, quantum simulations with ultracold atoms serve to understand the dynamics of complex quantum many-body systems [8, 10, 11]. One of the sources of complexity in these systems is the potential existence of quantum chaos induced by interactions and/or the presence of external fields.

Recently, many studies have focused on the understanding of the properties of interacting quantum systems that exhibit chaos. In particular, systems described by a regular Bose-Hubbard model are known to present a chaotic phase in their spectrum that appears as a function of the bosonic interaction strength [17, 22, 23, 24, 25, 27]. However, although it has been observed that quantum chaos in the Bose-Hubbard Hamiltonian persists in the presence of an external static field [3], a characterization of the chaotic phase as a function of interaction and tilt strengths is still lacking in literature.

1.2 Objectives and thesis structure

The aim of this thesis is to do a characterization of the chaotic phase of the tilted Bose-Hubbard Hamiltonian. We are interested in finding the evolution of such phase with the system parameters, in addition to finding the relations between such parameters that maximize the presence of chaos. For this task, we benchmark our results against the theoretical predictions of Random Matrix Theory.

In Chapter 2, the second quantization formalism is presented. Creation and annihilation operators are defined, and their relations and properties are shown. Also, the Bose-Hubbard Hamiltonian is introduced and its terms are explained, as well as its symmetries. Finally, a few ideas of quantum chaos are developed as well as how spectrum properties and eigenvectors structure are related to such phenomenon.

In Chapter 3, the three limits of the Bose-Hubbard Hamiltonian that admit analytical solutions are discussed and used in order to explain some physical properties of the system.

In Chapter 4, we present the process by which the Hamiltonian matrix can be obtained using a Bose-Hubbard system consisting of 2 bosons and 2 sites and another one formed by 3 bosons and 3 sites. Using the second system, we present the evolution of its eigenenergies with the tilt strength for different intensities of the particle interaction, observing the emergence of *avoided crossings*. The latter phenomenon is explained and its implications for the eigenstates are deduced.

We make use of a system made of 5 bosons and 5 sites to learn about the evolution of the spectrum as a function of the ratio J/U. Then, we carry out a detailed characterization of the chaotic phase using larger systems. Such characterization is done by comparing

the mean value of the *level spacing ratio* against Random Matrix Theory predictions. In addition, the *first generalized fractal dimension* is used to obtain information about the structure of the eigenstates within the chaotic regime. These simulations are done firstly fixing the tilt strength (in units of the interaction energy) and varying the tunneling term (also in units of the interaction energy), and secondly fixing the interaction energy measured in units of the tunneling energy, then varying the tilt term (also in units of the tunneling energy). The results of such simulations used to obtain the width of the chaotic phase, and the relations between the three parameters that maximize it.

Additionally, we analyze the entrance into the chaotic phase from the perspective of a particular Fock state that is typically used in experimental dynamical studies with cold atoms.

The last part of Chapter 4 presents the analysis of the scaling of the mean value and variance of the first generalized fractal dimension with the size of the Hilbert space and its comparison against Random Matrix Theory predictions.

Lastly, in Chapter 5, the most important conclusions drawn from the results of the simulations are summarized.

2 | Formalism

2.1 Quantum description of systems with N indistinguishable bosons

In order to study many-body problems, a formalism known as *second quantization* is used. This formalism makes use of operators, which can create or destroy particles in certain single-particle states, to build states an observables [4].

In order to introduce this formalism, a system formed by N identical bosons located in L single-particle states denoted by $|\varphi_i\rangle$ is considered. These single-particle states constitute a basis of the Hilbert space for each boson.

Many-particle states are given by the kets of occupation numbers

$$|n_1, n_2, ...n_L\rangle, \tag{2.1}$$

which indicate that there are n_i bosons in the single particle state $|\varphi_i\rangle$.

As we want these kets to form an orthonormal basis of the total Hilbert space and we want the total number of bosons to be preserved, they must fulfill the following properties:

- Normalization:

$$\langle n'_1, n'_2, ..., n'_L | n_1, n_2, ..., n_L\rangle = \delta_{n'_1,n_1}\delta_{n'_2,n_2}...\delta_{n'_L,n_L}. \tag{2.2}$$

- Completeness relation:

$$\sum_{n_1,n_2,...,n_L} |n_1, n_2, ..., n_L\rangle\langle n_1, n_2, ..., n_L| = \mathbb{1}. \tag{2.3}$$

- Preservation of the total number of bosons:

$$\sum_{i=1}^{L} n_i = N \tag{2.4}$$

  for any ket.

Once we have a way to build an orthonormal basis of the total Hilbert space, we can start discussing the *second quantization formalism*. As it was mentioned previously, it makes use of operators that can create or destroy particles in the individual single-particle states. Let us denote by b_l the operator that destroys a boson on the $|\varphi_l\rangle$ state, and $b_l^\dagger$ the operator that creates a boson on the $|\varphi_l\rangle$ state. These operators are known as *annihilation and creation operators*, respectively. In order to work with them, one must specify an algebra

of commutation relations, which in the bosonic case reads

$$[b_l, b_k] = [b_l^\dagger, b_k^\dagger] = 0, \tag{2.5}$$

$$[b_l, b_k^\dagger] = \delta_{l,k}. \tag{2.6}$$

Equations (2.5) and (2.6) show that operators regarding different single-particle states always commute, whereas operators for the same single-particle state only commute when they both create or annihilate bosons.

Having defined these operators, there is one other that can be built immediately from them, the *number operator*,

$$\hat{n}_l \equiv b_l^\dagger b_l. \tag{2.7}$$

Let us denote by n_l and $|n_l\rangle$ the eigenvalues and eigenstates of $\hat{n}_l$,

$$\hat{n}_l|n_l\rangle = n_l|n_l\rangle. \tag{2.8}$$

The latter operator has a relevant meaning: It gives the number of bosons that occupy the l-th single-particle state. In order to show this, a manipulation using the creation/annihilation operators is needed.

Starting from Eq. (2.7) yields

$$\hat{n}_l b_l|n_l\rangle = b_l^\dagger b_l b_l|n_l\rangle.$$

Now, using Eq. (2.6)

$$b_l^\dagger b_l b_l|n_l\rangle = (b_l b_l^\dagger - [b_l, b_l^\dagger])b_l|n_l\rangle = (b_l b_l^\dagger - \mathbb{1})b_l|n_l\rangle = b_l b_l^\dagger b_l|n_l\rangle - b_l|n_l\rangle.$$

Applying Eqs. (2.7) and (2.8), one has

$$b_l b_l^\dagger b_l|n_l\rangle - b_l|n_l\rangle = b_l\hat{n}_l|n_l\rangle - b_l|n_l\rangle = b_l n_l|n_l\rangle - b_l|n_l\rangle = (n_l - 1)b_l|n_l\rangle.$$

Therefore, we have proved that

$$\hat{n}_l b_l|n_l\rangle = (n_l - 1)b_l|n_l\rangle.$$

This means that $b_l|n_l\rangle$ is an eigenvector of the number operator, and its eigenvalue equals $(n_l - 1)$. This indicates that $b_l|n_l\rangle$ has to be proportional to the $|n_l - 1\rangle$ state. Thus

$$b_l|n_l\rangle = \mathcal{N}|n_l - 1\rangle.$$

Imposing that the state $b_l|n_l\rangle$ must be normalized yields

$$|\mathcal{N}|^2\langle n_l - 1|n_l - 1\rangle = 1 = \langle n_l|b_l^\dagger b_l|n_l\rangle = \langle n_l|\hat{n}_l|n_l\rangle = n_l\langle n_l|n_l\rangle = n_l,$$

since Eq. (2.2) dictates that $\langle n_l|n_l\rangle = 1$. Then

$$|\mathcal{N}| = \sqrt{n_l}.$$

Therefore, we can conclude

$$b_l|n_l\rangle = \sqrt{n_l}|n_l - 1\rangle. \tag{2.9}$$

Now we know how b_l acts on the state $|n_l\rangle$.

An analogous reasoning leads to

$$b_l^\dagger |n_l\rangle = \sqrt{n_l + 1}|n_l + 1\rangle. \tag{2.10}$$

Hence, taking n_l as the number of bosons in state $|\varphi_l\rangle$, one can state that b_l is the operator that destroys a boson on site l and $b_l^\dagger$ is the one that creates it.

In order to ensure that we have no chance of having a negative number of bosons on any single particle state, the annihilation operator must verify

$$b_l|0\rangle = 0. \tag{2.11}$$

This requirement is ensured by the fact that the eigenvalues of $\hat{n}_l$ can only be non-negative since

$$b_l|\varphi\rangle = |\varphi'\rangle \Rightarrow \langle\varphi|\hat{n}_l|\varphi\rangle = \langle\varphi|b_l^\dagger b_l|\varphi\rangle = \langle\varphi b_l|b_l\varphi\rangle = \langle\varphi'|\varphi'\rangle \geq 0.$$

Consequently, in view of Eq. (2.9) the eigenvalues of $\hat{n}_l$ must be integers, and condition (2.11) is fulfilled. Indeed, n_l can be interpreted as the number of bosons in the $|n_l\rangle$ state.

Once the basic operator formalism has been built, it can be concluded that the kets in Eq. (2.1) can be constructed as the tensor product of the eigenstates of the number operators,

$$|n_1, n_2, ..., n_L\rangle = |n_1\rangle \otimes |n_2\rangle \otimes ... \otimes |n_L\rangle, \tag{2.12}$$

and these kets receive the name of *Fock states*. The creation/annihilation and number operators act on Fock states as

$$\begin{aligned}
b_l|n_1, n_2, ..., n_L\rangle &= \sqrt{n_l}|n_1, n_2, ..., n_l - 1, ..., n_L\rangle, \\
b_l^\dagger|n_1, n_2, ..., n_L\rangle &= \sqrt{n_l + 1}|n_1, n_2, ..., n_l + 1, ..., n_L\rangle, \\
\hat{n}_l|n_1, n_2, ..., n_L\rangle &= n_l|n_1, n_2, ..., n_l, ..., n_L\rangle.
\end{aligned}$$

2.2 The Bose-Hubbard Hamiltonian

The Bose-Hubbard Hamiltonian is a simple model used to describe a system of N interacting bosons on L single-particle modes [5, 19]. The standard form of this Hamiltonian reads

$$\hat{H}_{BH} = -J \sum_{l=1}^{L-1} (\hat{b}_{l+1}^\dagger \hat{b}_l + \hat{b}_l^\dagger \hat{b}_{l+1}) + \frac{U}{2} \sum_{l=1}^{L} \hat{n}_l(\hat{n}_l - 1) + \sum_{l=1}^{L} \epsilon_l \hat{n}_l, \tag{2.13}$$

which has three terms that can be described as follows:

- Tunneling.

  This corresponds to the first term of the Hamiltonian. It indicates that bosons are allowed to tunnel to adjacent single-particle modes. This tunneling processes are characterized by an energy $J>0$.

- Interaction.

  The interaction is given by the second term, and shows that pairs of bosons occupying the same single-particle mode interact with an interaction energy U.

- Energy of single-particle modes

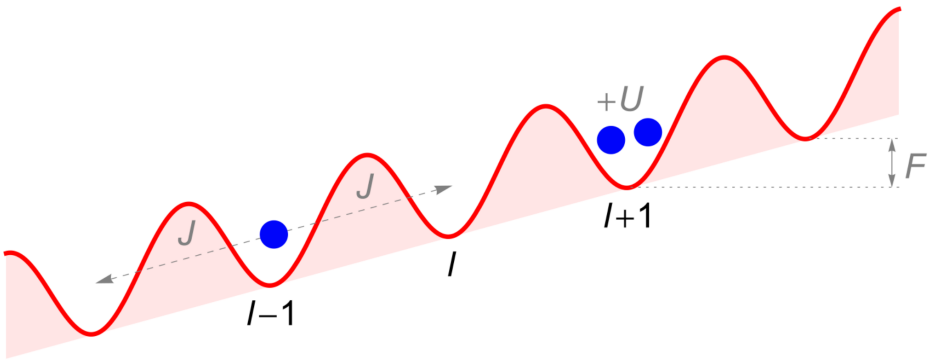

Figure 2.1: Schematic representation of the tilted Bose-Hubbard model, taken from [28].

The third term accounts for the energy of the single-particle modes: The l-th mode has energy ϵ_l, and gets multiplied by the number of bosons on that mode. However, as ϵ_l is usually the same for all modes and the number of bosons remains constant, the whole term is just a constant. Consequently, it can be removed from the Hamiltonian without missing any information.

For example, this Hamiltonian can describe a system of bosons in a lattice potential. In this realization, the single-particle modes correspond to states localized on the different sites of the lattice, called the *Wannier states*.

Having described these three usual terms, it should be remarked that an extra term is going to be considered throughout the work. As Fig. 2.1 shows, this additional term will describe the effect of an external static field (determined by a parameter F), which is symmetric with respect to the centre of the lattice. Adding this new part to the Hamiltonian, one obtains

$$\hat{H} = -J\sum_{l=1}^{L-1}(\hat{b}_{l+1}^{\dagger}\hat{b}_l + \hat{b}_l^{\dagger}\hat{b}_{l+1}) + \frac{U}{2}\sum_{l=1}^{L}\hat{n}_l(\hat{n}_l - 1) + F\sum_{l=1}^{L}\tilde{l}\hat{n}_l, \tag{2.14}$$

where

$$\tilde{l} \equiv l - \frac{L+1}{2} \tag{2.15}$$

indexes each site with respect to the center of the lattice. The last term of Eq. (2.14) describes a tilt of the lattice, as it changes linearly the energy of the single-particle Wannier states depending on their position across the lattice.

It can therefore be seen that the tilted Bose-Hubbard Hamiltonian (2.14) is fully specified by the parameters F, J, U, N and L. If preferred, instead of using both N and L, one can use one of them and the particle density n, defined as

$$n \equiv N/L. \tag{2.16}$$

Additionally, there is something that has to be specified in order to study the Hamiltonian: The boundary conditions. There are two valid options. The first one is using Periodic Boundary Conditions (PBC). This condition establishes a ring geometry over the system. It connects sites 1 and L [see Fig. 2.2(a)]. The second one consists in considering Hard Wall Boundary Conditions (HWBC), which connects sites 1 and L to a *wall*. Consequently, no tunneling is allowed between sites 1 and L. Figure 2.2(b) shows that sites 1 and L are not connected.

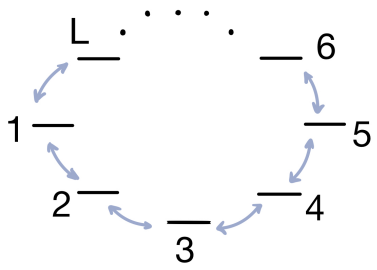

(2.2(a)) Periodic boundary conditions, which are equivalent to ring geometry.

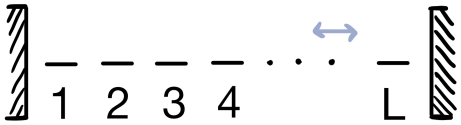

(2.2(b)) Hard-wall boundary conditions.

Figure 2.2: Possible boundary conditions for the Bose-Hubbard Hamiltonian.

Having understood the meaning of the Bose-Hubbard Hamiltonian and its parameters, we proceed to discuss its main symmetries.

- Total particle number conservation

  The total particle number operator is defined as

  $$\hat{N} = \sum_{l=1}^{L} \hat{n}_l. \tag{2.17}$$

  It can be proved that it commutes with the Hamiltonian and, consequently, its expectation value $\langle \hat{N} \rangle$ remains constant.

- Time-reversal symmetry

  The Hamiltonian matrix is real and symmetric. This implies that the Hamiltonian is invariant under the action of time-reversal operator, $\hat{T}$.

- Parity symmetry

  The Bose-Hubbard Hamiltonian is invariant under reflection symmetry, but only in the case where the external tilt is zero (this is intuitive, since adding a tilt term breaks the lattice symmetry, as it assigns different energies to the sites depending on their position with respect to the center and, consequently, a reflection will not leave the system invariant). The *parity operator* Π is defined as follows,

  $$\Pi |n_1, n_2, ..., n_L\rangle = |n_L, n_{L-1}, ..., n_2, n_1\rangle. \tag{2.18}$$

  If a Hamiltonian is invariant under the action of the parity operator, then it must verify

  $$\Pi H \Pi^\dagger = H. \tag{2.19}$$

  It can be seen that the parity operator is unitary,

  $$\Pi \Pi^\dagger = \mathbb{1}. \tag{2.20}$$

  Hence, combining equations (2.19) and (2.20), one can see that if H is invariant under the action of Π, then $[H, \Pi] = 0$.

  Therefore, one has to prove that the Hamiltonian (without the tilt term) commutes with the parity operator. In order to show this, it is convenient to define the action

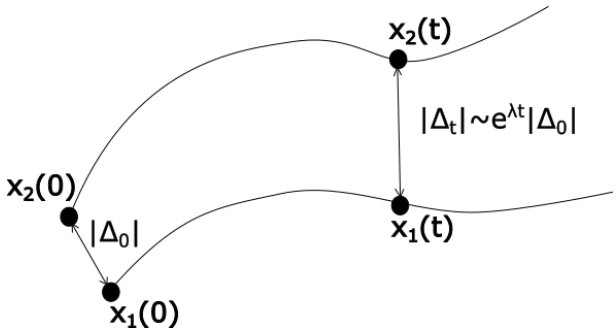

Figure 2.3: Pictorial evolution of the system in phase space for two close initial conditions.

of the parity operator on the creation/annihilation operators. In fact, this is just another way of defining the parity operator, instead of defining the action on the Fock states,

$$\Pi b_j^{(\dagger)} \Pi^\dagger = b_{L-j+1}^{(\dagger)}. \tag{2.21}$$

Thus,

$$\Pi \hat{n}_j \Pi^\dagger = \hat{n}_{L-j+1}. \tag{2.22}$$

It is then straightforward to check that

$$\Pi \hat{H}_{HB} \Pi^\dagger = \hat{H}_{HB}. \tag{2.23}$$

2.3 Quantum chaos: Spectral and eigenvector properties

A classical system is said to be chaotic when its dynamical evolution in phase space has an exponential sensitivity to the initial conditions [21]. Let us consider a system with two different initial conditions, but close to each other. One can name these two initial conditions in phase space $\boldsymbol{X_1}(0)$ and $\boldsymbol{X_2}(0)$, and one can also define their difference as $\boldsymbol{\Delta}_0 \equiv \boldsymbol{X_2}(0) - \boldsymbol{X_1}(0)$. Then, the system evolves from $t = 0$ (initial conditions) to an arbitrary later time t, where the coordinates in phase space will be $\boldsymbol{X_1}(t)$ and $\boldsymbol{X_2}(t)$. In order to see if the system exhibits chaotic behaviour, one needs to assess if the trajectories $\boldsymbol{X_1}(t)$ and $\boldsymbol{X_2}(t)$ depart from each other exponentially in time. In order to study this behaviour, the *Lyapunov exponent* λ is used, defined as

$$\lambda = \lim_{\substack{t\to\infty \\ ||\boldsymbol{\Delta_0}||\to 0}} \frac{1}{t} \log \frac{||\boldsymbol{\Delta_t}||}{||\boldsymbol{\Delta_0}||}, \tag{2.24}$$

where $\boldsymbol{\Delta_t} = \boldsymbol{X_2}(t) - \boldsymbol{X_1}(t)$. Figure 2.3 shows pictorially the evolution of the dynamics of the system for two different (but close) initial conditions, and marks the difference between the positions of the system in phase space after a time t.

Definition (2.24) leads to the conclusion that $\lambda > 0$ implies classical chaotic dynamics. However, one must take into account the fact that the exponential growth of the distance $||\boldsymbol{\Delta_t}||$ will be bounded by the size of phase space.

Therefore, a *chaotic classical system* will show an unpredictable evolution for arbitrarily small uncertainty in the initial conditions. On the other hand, a classical system is said

to be a *regular system* when its dynamics are not chaotic. In fact, most systems will not show a fully chaotic or fully regular behaviour but rather a mixed behaviour, exhibiting chaotic and regular regions in phase space.

A definition of chaos in classical systems has been given, but the interest now is extending this definition to quantum systems. Here, we encounter a problem. The given definition cannot be used for quantum systems. The issue lies in considering two initial conditions arbitrarily close. This is not possible for quantum systems, as Heisenberg uncertainty principle divides the phase space into cells of a minimum area given by $\Delta x \Delta p \geq \hbar/2$. Consequently, it is not consistent to speak of an arbitrarily small distance between two initial conditions in phase space.

In order to avoid this problem, one could think of taking the classical limit (by making $\hbar \to 0$) of the quantum system and then studying the dynamics of such classical limit. Then, if the classical counterpart of the system exhibits chaotic behaviour, the quantum system could be chaotic. However, this is not so easy to do, as taking such limit is not trivial and, in fact, many systems do not even have a well-defined classical limit.

For those quantum systems for which a fully chaotic classical limit can be found, statistical properties of the energy spectrum were shown to be in agreement with the Gaussian ensembles of *Random Matrix Theory* [12]. On the other hand, for those systems for which a fully regular classical limit can be found, spectral properties are given by Poissonian statistics.

Hence, the existence of spectral properties in agreement with Random Matrix Theory has been taken as the definition of quantum chaos [12].

Let us discuss some basic concepts of Random Matrix Theory and its spectral properties. A random matrix is a matrix whose entries (or at least some of them) are random numbers. Among all the different sets of matrices that can be defined, Gaussian ensembles are specially interesting. The matrix elements of Gaussian ensembles are statistically independent and described by Gaussian distributions. Each ensemble is invariant under certain symmetry transformations. There are three types of Gaussian ensembles:

- Gaussian Orthogonal ensemble (GOE)
- Gaussian Unitary ensemble (GUE)
- Gaussian Simplectic ensemble (GSE)

Only the Gaussian Orthogonal ensemble will be relevant for us. It is formed by a set of real and symmetric matrices h, which are invariant under orthogonal transformations. The entries of the matrices are random elements drawn from a Gaussian distribution with

$$\mu(h_{ij}) = 0, \quad \sigma^2(h_{ij}) = 1 + \delta_{ij}, \tag{2.25}$$

where μ and σ denote, respectively, the mean and the standard deviation.

Given the eigenvalues E_n of a GOE matrix, the level spacing can be defined as

$$s_n \equiv E_{n+1} - E_n, \tag{2.26}$$

and let $\Delta \equiv \langle s \rangle$ denote the average value of the level spacing over the full spectrum. Then, it can be shown that the distribution of the normalized level spacing, $\tilde{s} = s/\Delta$ is the following

$$P_{GOE}(\tilde{s}) = \frac{\pi}{2} \tilde{s} e^{-\tilde{s}^2 \pi/4}. \tag{2.27}$$

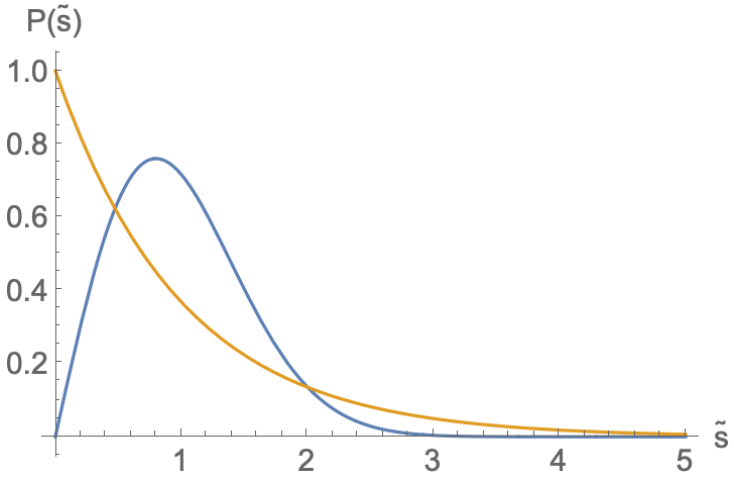

Figure 2.4: Level spacing distributions corresponding to the Wigner surmise [blue, Eq. (2.27)] and the Poisson distribution [yellow, Eq. (2.28)].

The latter distribution is called the *Wigner surmise*, which is characterized by level repulsion at $\tilde{s} = 0$.

In contrast, if the eigenvalues of a matrix were distributed according to Poissonian statistics, one may see that

$$P_{Poisson}(\tilde{s}) = e^{-\tilde{s}}, \tag{2.28}$$

where the level repulsion at $\tilde{s} = 0$ is absent. Both distributions are represented in Fig. 2.4.

Therefore, by evaluating $P(\tilde{s})$ for a quantum system, and by comparing it against (2.27), one may conclude if quantum chaos is present. However, it is important to remark something at this point. If one wants to compare against the Wigner distribution, only subspaces of the Hilbert space with no remaining symmetries must be considered.

In order to compare against Random Matrix Theory, instead of the level spacings it is more convenient to consider the level spacing ratio

$$r_n \equiv \min\left\{\frac{s_n}{s_{n+1}}, \frac{s_{n+1}}{s_n}\right\}. \tag{2.29}$$

It is known that [7]

$$\langle r_{GOE}\rangle = 0.5307, \quad \langle r_{Poisson}\rangle = 2\log 2 - 1 \approx 0.3867. \tag{2.30}$$

Therefore, if the energy spectrum of a system is known, then so is the level spacing and, consequently, the level spacing ratio. Hence, comparison against the values in Eq. (2.30) is a way to determine if quantum chaos is present.

Besides the energy spectrum, other properties of the system can inform about the presence of chaos, such as the structural properties of eigenvectors. Particularly, for the case of the Bose-Hubbard Hamiltonian, it has been observed that within the chaotic regime eigenvectors become fully extended in Fock space in the thermodynamic limit [22, 23, 24, 25], in agreement also with the predictions of Random Matrix Theory for the eigenvectors. Moreover, all eigenstates share the same structural properties.

Let us describe how the analysis of the eigenstate features can be done. First of all, it is necessary to define the concept of *generalized fractal dimensions*. Let us consider a state

$|\varphi\rangle$ expanded on a basis $|\alpha\rangle$ in a Hilbert space of size $\mathcal{D}$,

$$|\varphi\rangle = \sum_\alpha \varphi_\alpha |\alpha\rangle, \quad \sum_\alpha |\varphi_\alpha|^2 = 1. \tag{2.31}$$

Then the R_q moments of the set of intensities $|\varphi_\alpha|^2$ are defined as

$$R_q = \sum_\alpha |\varphi_\alpha|^{2q}, \quad q \in \mathbb{R}. \tag{2.32}$$

The generalized fractal dimensions D_q are given by

$$D_q = \lim_{\mathcal{D}\to\infty} \frac{1}{1-q} \frac{\log(R_q)}{\log(\mathcal{D})} \equiv \lim_{\mathcal{D}\to\infty} \tilde{D}_q(\mathcal{D}), \tag{2.33}$$

where $\tilde{D}_q$ is known as the *finite-size generalized fractal dimension*. The quantities D_q determine the scaling exponent of the R_q moments with the size of Hilbert space,

$$R_q \underset{\mathcal{D}\to\infty}{\sim} \mathcal{D}^{-(q-1)D_q}. \tag{2.34}$$

The values of D_q give us information about the structure of the state $|\varphi\rangle$ in the basis $|\alpha\rangle$.

For the case of a fully extended state, one has that all the coefficients of the linear combination must be the same. As $\sum_\alpha |\varphi_\alpha|^2 = 1$ and we are assuming a dimension $\mathcal{D}$ of the Hilbert space, then $|\varphi_\alpha| = 1/\sqrt{\mathcal{D}}$. Using the previous definition,

$$R_q = \sum_\alpha |\varphi_\alpha|^{2q} = \sum_\alpha \left(\frac{1}{\mathcal{D}}\right)^q = \mathcal{D}\left(\frac{1}{\mathcal{D}}\right)^q = \mathcal{D}^{1-q}, \tag{2.35}$$

and from Eq. (2.34) it ensues

$$D_q = 1 \quad \forall q. \tag{2.36}$$

Hence, we have proved that those states that are fully extended have a generalized fractal dimension D_q equal to 1, independently of the value of q.

A similar reasoning can be done for a localized state. In this case, only one a fixed finite number of coefficients φ_α in the linear expansion are non-zero. This implies that the moments R_q do not change with the size of Hilbert space. Hence, from Eq. (2.34),

$$R_q \underset{\mathcal{D}\to\infty}{\sim} \mathcal{D}^0 \Rightarrow D_q = 0 \quad \forall q. \tag{2.37}$$

These are the two limiting cases for the states, but generally one may not have a fully extended or localized state. Then, the value of D_q will vary with q, giving a *multifractal state*.

Consequently, analyzing the generalized fractal dimensions of the eigenstates one can conclude whether they become fully extended, fully localized or multifractal and also assess the emergence of quantum chaos.

3 | Analytical limits of the Bose-Hubbard Hamiltonian

The tilted Bose-Hubbard Hamiltonian can be solved analytically only in the cases $J = 0$, $U = 0$ and $U = F = 0$. The study of these three cases is shown in the following sections. It should be remarked that hard-wall boundary conditions are assumed for the two first cases, whereas for the third one the case $L = \infty$ is considered.

3.1 Case $U = F = 0$

In the absence of interaction and tilt, Hamiltonian (2.14) is reduced to the tunneling term

$$\hat{H}_{U=F=0} = -J \sum_{j=1}^{L-1} (\hat{b}_{j+1}^{\dagger} \hat{b}_j + \hat{b}_j^{\dagger} \hat{b}_{j+1}). \tag{3.1}$$

Solving this case requires a change of basis in the creation/annihilation operators, i.e., we use a different set of single-particle modes,

$$d_k^{(\dagger)} := \sqrt{\frac{2}{L+1}} \sum_{j=1}^{L} \sin\left(\frac{\pi k j}{L+1}\right) b_j^{(\dagger)}, \quad k = 1, ..., L, \tag{3.2}$$

where operator $d_k^{(\dagger)}$ destroys (creates) a boson in a standing-wave single-particle state with $k + 1$ nodes.

The initial creation/annihilation operators can be written as linear combinations of the new ones,

$$b_j^{(\dagger)} = \sqrt{\frac{2}{L+1}} \sum_{k=1}^{L} \sin\left(\frac{\pi k j}{L+1}\right) d_k^{(\dagger)}, \quad j = 1, ..., L. \tag{3.3}$$

The latter relation can be insterted in (3.1) leading to

$$H = -2J \sum_{k=1}^{L} \cos\left(\frac{\pi k}{L+1}\right) d_k^{\dagger} d_k. \tag{3.4}$$

The eigenstates are then the Fock states for the new operators $\hat{\hat{n}}_k \equiv d_k^{\dagger} d_k$, and the many-body energies can be constructed from the single-particle energies

$$E_k \equiv -2J \cos\left(\frac{\pi k}{L+1}\right), \quad k = 1, ..., L. \tag{3.5}$$

In the limit $U = F = 0$, the many-particle energy levels are heavily degenerate, since the

occupation of different sets of single-particle modes can yield the same total energy.

3.2 Case $J = 0$

In this limit, the Hamiltonian reads

$$\hat{H}_{J=0} = \frac{U}{2}\sum_{j=1}^{L}\hat{n}_j(\hat{n}_j - 1) + F\sum_{j=1}^{L}\tilde{j}\hat{n}_j, \tag{3.6}$$

whose eigenstates are the Fock states of the on-site densities, $|\boldsymbol{n}\rangle \equiv |n_1, n_2, ..., n_L\rangle$. In this case, the modes are decoupled, and the bosons are localized at different sites of the lattice. It can be straightforwardly seen that

$$E_{|\boldsymbol{n}\rangle} = \frac{U}{2}\sum_{j=1}^{L}n_j^2 + F\sum_{j=1}^{L}jn_j - \frac{L+1}{2}FN - \frac{U}{2}N. \tag{3.7}$$

From the latter expression, one can see that certain Fock states may be degenerate for certain values of U and F.

3.3 Case $U = 0$

Even in the case where the tilt term is present, the non-interacting case has an analytical solution. In Ref. [14], a detailed study of the eigenstates and eigenenergies of the model is presented. Here, we give a summary of the basic steps to build the solution.

In this case, the limit $L \to \infty$ is assumed, with periodic lattice potential of period d. The single-particle Hamiltonian can be written as

$$H = \frac{p^2}{2M} + V(x) + Fx, \quad V(x+d) = V(x). \tag{3.8}$$

Figure 3.1 shows a schematic illustration of the potential $\cos(x) + Fx$. In terms of the bandwidth energy Δ of the periodic potential, the Hamiltonian (in the Wannier states basis $|j\rangle$) takes the form

$$H = -\frac{\Delta}{4}\sum_{j=-\infty}^{\infty}(|j\rangle\langle j+1| + |j+1\rangle\langle j|) + Fd\sum_{j=-\infty}^{\infty}j|j\rangle\langle j|. \tag{3.9}$$

Alternatively, one can use a representation in Bloch waves $|k\rangle$

$$|k\rangle = \sum_{j=-\infty}^{\infty}|j\rangle\langle j|k\rangle = \sqrt{\frac{d}{2\pi}}\sum_{j=-\infty}^{\infty}|j\rangle e^{ijkd}, \quad k \in \left[\frac{-\pi}{d}, \frac{\pi}{d}\right]. \tag{3.10}$$

One can see that Hamiltonian (3.9) is diagonal in this basis, $\langle k'|H|k\rangle = d\delta(k'-k)H(k)$, with

$$H(k) = -\frac{\Delta}{2}\cos(kd) + iF\frac{d}{dk}. \tag{3.11}$$

The eigenstates $|\psi_m\rangle$ of the system can be straightforwardly obtained by solving the differential equation

$$-\frac{\Delta}{2}\cos(kd)|\varphi\rangle + iF\frac{d}{dk}|\varphi\rangle = E|\varphi\rangle, \tag{3.12}$$

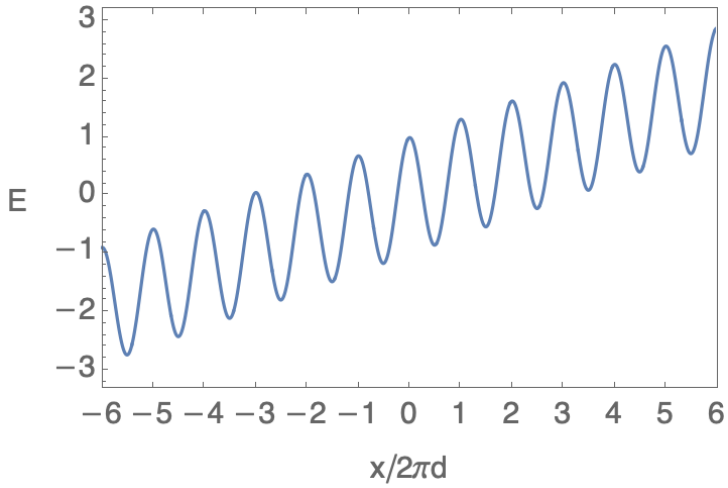

Figure 3.1: Periodic potential of period d with a tilt term Fx, for $Fd = 0.05$.

with the periodic boundary condition $\psi(k) = \psi(k+b)$, with $b = 2\pi/d$, the length of the first Brillouin zone. This leads to

$$\psi(k) = \sqrt{\frac{d}{2\pi}} e^{-i[Ek + \Delta \sin(kd)/(2d)]/F}, \tag{3.13}$$

and

$$\frac{Eb}{F} = 2\pi m \Rightarrow E = mFd, \quad m = 0, \pm 1, ... \tag{3.14}$$

which form the so-called *Wannier-Stark ladder*.

Using a Fourier transform, the description of the eigenstates in terms of the Wannier basis is possible

$$\psi_m(n) = \langle n|\psi_m\rangle = \int_{-b/2}^{b/2} dk \langle n|k\rangle\langle k|\psi_m\rangle = \frac{d}{2\pi}\int_{-b/2}^{b/2} dk e^{i[(n-m)kd - \Delta \sin(kd)/2dF]} \tag{3.15}$$

$$= \frac{1}{2\pi}\int_{-\pi}^{\pi} du e^{i[(n-m)u - \Delta \sin(u)/2dF]} = J_{n-m}\left(\frac{\Delta}{2dF}\right), \tag{3.16}$$

where J denotes the Bessel function. This provides the *Wannier-Stark states* in the Wannier representation

$$|\psi_m\rangle = \sum_n J_{n-m}\left(\frac{\Delta}{2dF}\right)|n\rangle. \tag{3.17}$$

3.4 Some physical properties of the Bose-Hubbard Hamiltonian

There is an interesting property of the Bose-Hubbard Hamiltonian in the absence of tilt that can be qualitatively described from the already explained analytical limits: The ground state phase transition from a superfluid to a Mott insulator at integer values of the density.

The ground state of the Bose-Hubbard Hamiltonian takes a different form depending on the relation between the Hamiltonian parameters. In the limit $U/J \gg 1$, one may neglect the tunneling term from the Hamiltonian and use the results of the second analytical

solution (Sec. 3.2 for $F = 0$). From Eq. (3.7), one can see that the state that minimizes $\sum_{j=1}^{L} n_j^2$ will be the ground state, which is the case of having n bosons per site,

$$|\phi_{gs}\rangle = |n, n, ..., n\rangle. \tag{3.18}$$

The energy of the ground state is

$$E_{gs} = L\frac{U}{2}n(n-1). \tag{3.19}$$

In this limit, tunneling is supressed since it is energetically unfavorable. For example, let us start from the ground state and let one boson tunnel, inducing an energy cost

$$\Delta E = \frac{U}{2}(n+1)n + \frac{U}{2}(n-1)(n-2) - 2\frac{U}{2}n(n-1) = U. \tag{3.20}$$

Since $U \gg J$, this energy increment is very high. Hence, matter flow across the system is suppressed, i.e., the high interaction value induces an insulating behaviour. The system forms a Mott insulator in this limit.

In the limit $U/J \ll 1$, the interaction part may be neglected and the first analytical solution (Sec. 3.1) can be used. In the lowest configuration all bosons occupy the momentum state with lowest energy,

$$|\varphi_{gs}\rangle = \frac{(d_l^\dagger)^N}{\sqrt{N!}}|0\rangle, \tag{3.21}$$

where $|0\rangle$ denotes the vacuum state, and the ground state energy reads

$$E_{gs} = -2JN. \tag{3.22}$$

Thus, each boson is delocalized over the whole lattice and, consequently, matter can flow across the system.

After finding the ground state in both limits, it can be reasoned that, in the thermodynamic limit, changing the ratio J/U the structure of the groud state changes from one insulating state to another state that exhibits good mass transport properties, i.e., in the thermodynamic limit, it can be seen that the ground state undergoes a phase transition at a critical value of J/U, between a Mott insulator an a superfluid phase.

These two phases also differ, for instance, in the on-site density fluctuations,

$$\mathrm{var}(\hat{n}_j) \equiv \langle \hat{n}_j^2 \rangle - \langle \hat{n}_j \rangle^2 \begin{cases} \sim n & \text{in the superfluid phase,} \\ \to 0 & \text{in the Mott insulator phase,} \end{cases} \tag{3.23}$$

with $n = \langle \hat{n}_j \rangle$. The superfluid to Mott insulator phase was first theoretically studied in Ref. [5]. Later, it was proposed to be experimentally investigated with cold atoms in Ref. [15]. It was experimentally observed for the first time in 2002 in a 3-D optical lattice [9], followed by an observation in one-dimensional lattices [29].

The critical value of J/U is dependent on the dimensionality and on the density. For example, for a one-dimensional lattice and a density $n = 1$, the critical J/U value is known to be

$$\left(\frac{J}{U}\right)_c \approx 0.3, \tag{3.24}$$

from both numerical simulations and experiments. A more detailed analysis of the phase

transition and its properties can be found in Ref. [20].

4 | Spectral and eigenvector features of the Bose-Hubbard Hamiltonian

In the previous chapter the analytical solutions for the limiting cases of the Bose-Hubbard Hamiltonian were studied. When $U \neq 0$ and also $J \neq 0$ there is no analytical solution (not even for the ground state) and, consequently, the investigation of its spectral and eigenvector properties must rely on numerical simulations.

In this chapter, some numerical simulations of the system are presented. All of them are made using a density $n = 1$, and make use of the on-site Fock state basis for the diagonalization of the Hamiltonian.

4.1 Building the Hamiltonian matrix. Example of spectra

The analysis of a system with a small number of bosons and sites is shown. In this part, the untilted Bose-Hubbard Hamiltonian is considered. This will serve to illustrate how the matrix of the Hamiltonian is constructed, as well as to discuss the properties of its energy spectrum.

We proceed now to diagonalize the Bose-Hubbard Hamiltonian. First of all, it is necessary to specify a basis of Hilbert space. One basis is provided by the Fock states of the on-site number operators $\hat{n}_l$, $|n_1, n_2, ..., n_L\rangle$. The size of this basis is given by the number of ways to distribute N identical bosons among L different modes,

$$\dim H = \binom{N + L - 1}{N}. \tag{4.1}$$

Hence, for a system with constant particle density, $\dim H$ grows exponentially with N or L. In order to illustrate this idea, some dimensions of the Hilbert space for a system with $n = 1$ are shown in Table 4.1.

Let us construct explicitly the Hamiltonian matrix for the particular case $L = N = 2$.

N	2	3	4	5	6	7	8	9	10	11	12
$\dim H$	3	10	35	126	462	1716	6435	24310	92378	352716	1352078

Table 4.1: Dimensions of the Hilbert space for different values of N, for a fixed density $n = 1$.

Using Eq. (4.1), one can see that $\dim H = 3$. We work in the on-site Fock state basis,

$$\{|20\rangle, |11\rangle, |02\rangle\}. \tag{4.2}$$

The matrix elements are given by $\langle\alpha|\hat{H}|\beta\rangle$, where $|\alpha\rangle$ and $|\beta\rangle$ are states of the considered basis. Since the Hamiltonian is self-adjoint, it is enough to evaluate its diagonal terms and upper diagonal part. Let us evaluate the kets $\hat{H}|\alpha\rangle$,

$$\hat{H}|20\rangle = -J(\hat{b}_2^\dagger\hat{b}_1 + \hat{b}_1^\dagger\hat{b}_2)|20\rangle + \frac{U}{2}\sum_{j=1}^{2}\hat{n}_j(\hat{n}_j - 1)|20\rangle = -J\sqrt{2}|11\rangle + U|20\rangle, \tag{4.3}$$

$$\hat{H}|11\rangle = -J(\hat{b}_2^\dagger\hat{b}_1 + \hat{b}_1^\dagger\hat{b}_2)|11\rangle + \frac{U}{2}\sum_{j=1}^{2}\hat{n}_j(\hat{n}_j - 1)|11\rangle = -J\sqrt{2}|02\rangle - J\sqrt{2}|20\rangle, \tag{4.4}$$

$$\hat{H}|02\rangle = -J(\hat{b}_2^\dagger\hat{b}_1 + \hat{b}_1^\dagger\hat{b}_2)|02\rangle + \frac{U}{2}\sum_{j=1}^{2}\hat{n}_j(\hat{n}_j - 1)|02\rangle = U|02\rangle - J\sqrt{2}|11\rangle. \tag{4.5}$$

Therefore, we have

$$H = \begin{pmatrix} U & -J\sqrt{2} & 0 \\ -J\sqrt{2} & 0 & -J\sqrt{2} \\ 0 & -J\sqrt{2} & U \end{pmatrix}. \tag{4.6}$$

After obtaining the Hamiltonian matrix, one can diagonalize it and get its eigenstates and eigenvalues. When doing so, one can learn from the properties of the energies and states of the system.

In order to explore the properties of the spectrum and eigenstates, a system with $N = L = 3$ ($\dim H = 10$) is used. The Hamiltonian matrix has been calculated using Mathematica, obtaining

$$\begin{pmatrix} 3U-3F & -\sqrt{3}J & 0 & 0 & 0 & 0 & 0 & 0 & 0 & 0 \\ -\sqrt{3}J & U-2F & -J & -2J & 0 & 0 & 0 & 0 & 0 & 0 \\ 0 & -J & U-F & 0 & -\sqrt{2}J & 0 & 0 & 0 & 0 & 0 \\ 0 & -2J & 0 & U-F & -\sqrt{2}J & 0 & -\sqrt{3}J & 0 & 0 & 0 \\ 0 & 0 & -\sqrt{2}J & -\sqrt{2}J & 0 & -\sqrt{2}J & 0 & -\sqrt{2}J & 0 & 0 \\ 0 & 0 & 0 & 0 & -\sqrt{2}J & F+U & 0 & 0 & -J & 0 \\ 0 & 0 & 0 & -\sqrt{3}J & 0 & 0 & 3U & -\sqrt{3}J & 0 & 0 \\ 0 & 0 & 0 & 0 & -\sqrt{2}J & 0 & -\sqrt{3}J & F+U & -2J & 0 \\ 0 & 0 & 0 & 0 & 0 & -J & 0 & -2J & 2F+U & -\sqrt{3}J \\ 0 & 0 & 0 & 0 & 0 & 0 & 0 & 0 & -\sqrt{3}J & 3F+3U \end{pmatrix}. \tag{4.7}$$

The spectrum of the system is also obtained using Mathematica. Figure 4.1 depicts the evolution of the energy levels as functions of F/U for different values of J/U. In the $J/U = 0$ case the Hamiltonian is diagonal in the chosen basis, and it was analytically solved in Sec. 3.2, where it was shown that the energy levels follow Eq. (3.7). It can be seen in the plot how the energy levels evolve linearly with F/U and how they cross at specific values of the tilt strength.

When $J/U \neq 0$, the matrix is no longer diagonal. It is noticeable that at the crossings for $J/U = 0$ the energy levels seem to repel each other when increasing the value of J/U, and exhibit *avoided crossings*. This is, the term that makes the real crossings become avoided crossings is the tunneling part. It can be seen that this repulsion is enhaced as J/U grows.

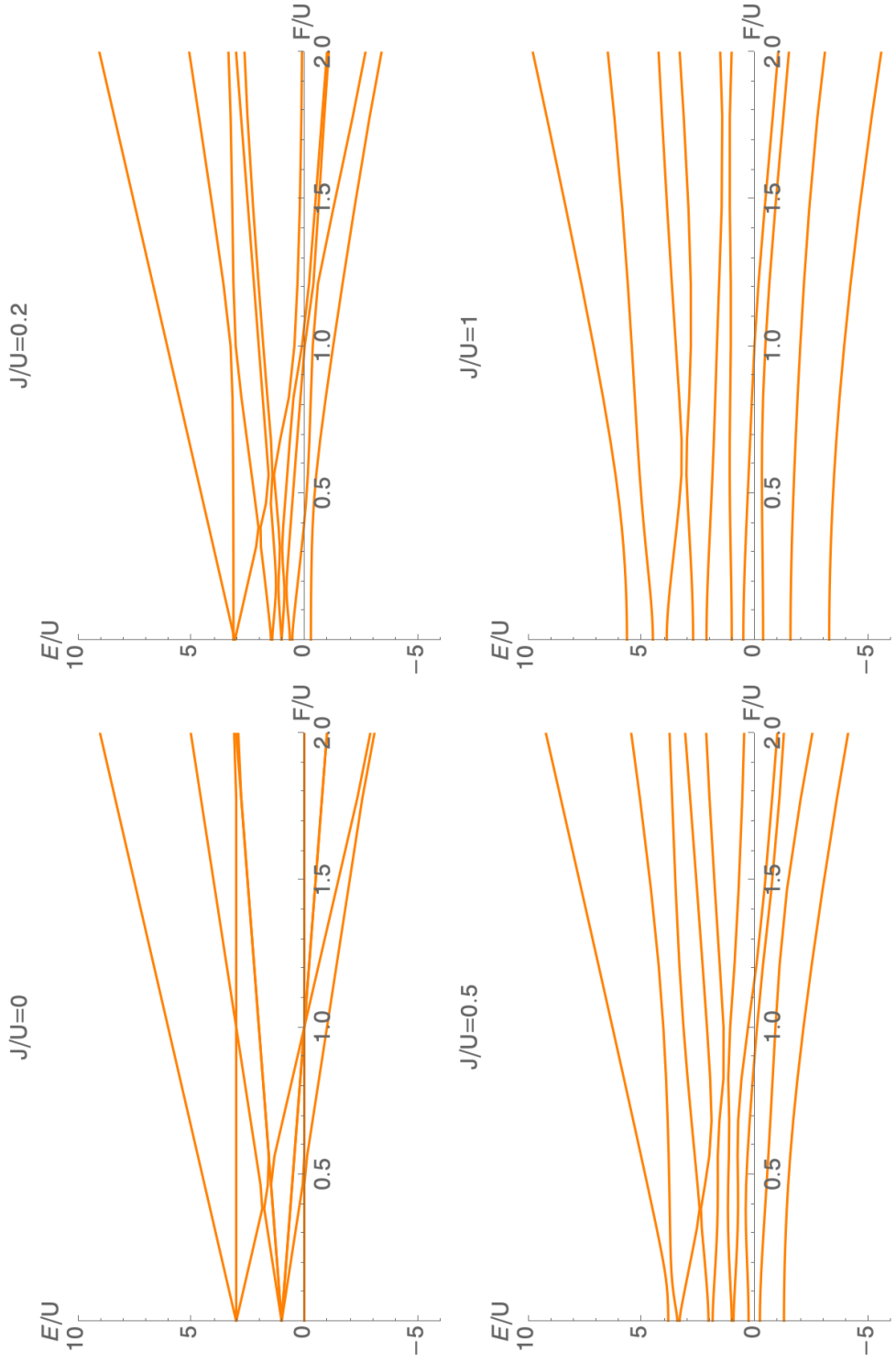

Figure 4.1: Evolution of the energy levels with F/U for $L = N = 3$, using different values of J/U.

4.2 Level repulsion: Avoided crossings

It has been shown that when the tunneling term of the Hamiltonian is non-zero a level repulsion between those states that exhibited a real crossing at $J/U = 0$ emerges. This phenomenon can be explained from the Hamiltonian matrix. The tunneling term is the one that contributes with off-diagonal terms. Therefore, in the most general case, the Hamiltonian can be written as the sum of two terms, one that is diagonal and one that is not,

$$H = H_0 + V, \tag{4.8}$$

where H_0 is the diagonal part, corresponding to the interaction and tilt terms, and V is the non-diagonal part, i.e., the tunneling term. In order to explain the emergence of avoided crossings, we start considering a small non-diagonal contribution (we consider a sufficiently small J). Then, one can see what happens when a perturbation is introduced to two states, $|\phi_1\rangle$ and $|\phi_2\rangle$, that exhibited a real crossing for the case $J = 0$. For small J, only the subspace spanned by the two states needs to be considered. Therefore, one can build the Hamiltonian of this subspace,

$$H_s = \begin{pmatrix} \varepsilon_1 & \langle\phi_1|V|\phi_2\rangle \\ \langle\phi_2|V|\phi_1\rangle & \varepsilon_2 \end{pmatrix}, \tag{4.9}$$

where $\varepsilon_1 = \langle\phi_1|H_0|\phi_1\rangle$ and $\varepsilon_2 = \langle\phi_2|H_0|\phi_2\rangle$. As it has been mentioned, the diagonal parts of the Hamiltonian follow from the interaction and tilt terms, and the off-diagonal ones come from the tunneling term. Hence, the matrix in Eq. (4.9) is a 2×2 matrix whose diagonal entries depend on the parameters U and F, and the off-diagonal ones depend on J. Renaming the matrix entries, Eq. (4.9) can be written as

$$H_s = \begin{pmatrix} a+b & c \\ c & a-b \end{pmatrix}, \tag{4.10}$$

where $a = a(U, F)$, $b = b(U, F)$ and $c = c(J)$ (note that it has already been imposed that the matrix is real, as it was already mentioned that it is invariant under time-reversal symmetry). Here, the two cases, $J = 0$ and $J \neq 0$, can be easily compared. Taking $J = 0$, one can see that

$$E_{1,2}(c = 0) = a \pm b. \tag{4.11}$$

Now, when $J \neq 0$,

$$E_{1,2}(c = 0) = a \pm \sqrt{b^2 + c^2}. \tag{4.12}$$

One can represent the eigenenergies as a function of b, as in Fig. 4.2. It can be observed that an increase of the value of c results in a separation of the two energies that previously showed a real crossing. In fact, one can see that the minimum value of the separation ΔE appears at $b = 0$, and it can be checked that $\Delta E_{min} = 2\,|c|$. Consequently, the minimum gap between two states that cross for $J = 0$ grows linearly with c, the off-diagonal part of the Hamiltonian matrix, i.e., the greater J is, the more noticeable the avoided crossing.

The eigenvectors of (4.10) read

$$|\psi_1\rangle = \cos(\theta/2)|\phi_1\rangle + \sin(\theta/2)|\phi_2\rangle, \tag{4.13}$$

$$|\psi_2\rangle = \sin(\theta/2)|\phi_1\rangle - \cos(\theta/2)|\phi_2\rangle, \tag{4.14}$$

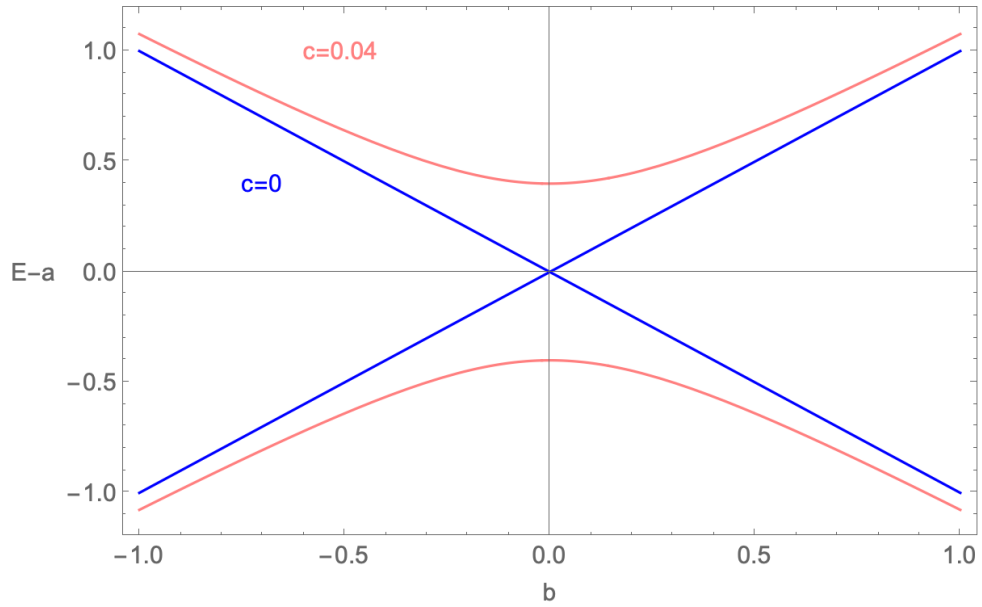

Figure 4.2: Evolution of the energy levels given in Eqs. (4.11) and (4.12). In blue, the eigenenergies when $c = 0$, exhibiting a real crossing. In pink, the same eigenenergies with $c = 0.04$, which undergo an avoided crossing.

where $\tan(\theta/2) = c/b$. In our case, θ parametrizes the change of F/U through the crossing. Fixing a $c \neq 0$ value, one can study the evolution of the eigenstates [27]

$$\frac{b}{c} \ll 0 \Rightarrow \theta \to \pi \Rightarrow \begin{cases} |\psi_1\rangle = |\phi_2\rangle, \\ |\psi_2\rangle = |\phi_1\rangle, \end{cases} \tag{4.15}$$

$$b = 0 \Rightarrow \theta \to \pi/2 \Rightarrow |\psi_{1,2}\rangle = \frac{1}{\sqrt{2}}[|\phi_1\rangle \pm |\phi_2\rangle], \tag{4.16}$$

$$\frac{b}{c} \gg 0 \Rightarrow \theta \to 0 \Rightarrow \begin{cases} |\psi_1\rangle = |\phi_1\rangle, \\ |\psi_2\rangle = -|\phi_2\rangle. \end{cases} \tag{4.17}$$

The evolution of $|\psi_{1,2}\rangle$ with b is given by a clockwise rotation of the unperturbed states $|\phi_{1,2}\rangle$. In the limit of very large $|b/c|$, the new eigenstates become proportional to the eigenstates of the unperturbed matrix. Note that at the avoided crossing ($b \to 0$) the eigenstates become a homogeneous superposition of the states $|\phi_{1,2}\rangle$, i.e., level repulsion implies strong mixing, and hence avoided crossings in the spectrum signal significant changes in the eigenstate structure.

4.3 Level dynamics

Equipped with the previous knowledge, we are now in a position to interpret the emergent properties in the spectrum of the system as N increases. Let us consider a system of 5 bosons and 5 sites, which has $\dim H = 126$, and monitor the level evolution, or *level dynamics* for $F = 0$ with the parameter J/U. Mathematica is used to obtain its eigenstates and eigenenergies. From this point, instead of working with the proper energies of the system, it is convenient to use the *rescaled energy*, defined as

$$\epsilon \equiv \frac{E - E_{min}}{E_{max} - E_{min}}. \tag{4.18}$$

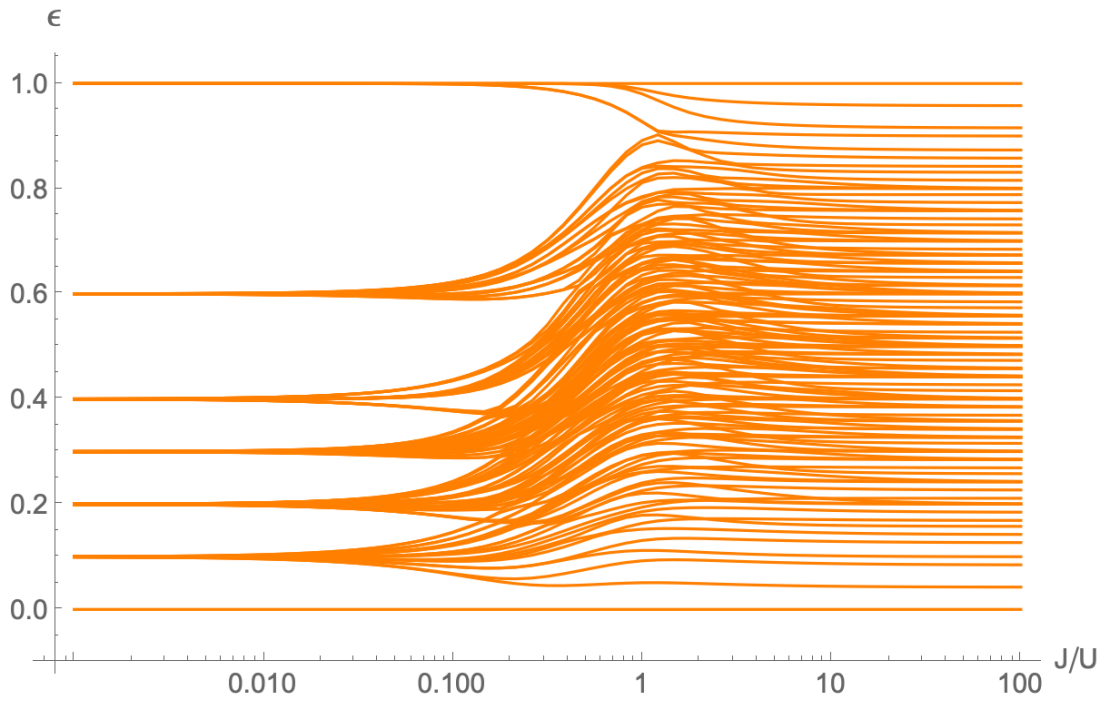

Figure 4.3: Evolution of the rescaled energies with J/U for $L = N = 5$, without tilt term.

For all the simulations of this chapter, unless otherwise indicated, we consider 61 equally spaced (in logarithmic scale) values of J/U going from 0.001 to 100.

The results for the simulation are depicted in Fig. 4.3, where it can be seen that, on the strongly interacting limit $J/U \ll 1$, the eigenenergies are heavily degenerate, and they approach the levels of Eq. (3.7) described in the analytical solution of Sec. 3.2. Hence, one can expect that (using $F = 0$) the eigenstates have an associated energy proportional to $\sum_{j=1}^{L} n_j^2$. On the opposite hand, in the non-interacting limit $J/U \gg 1$, one can observe that the energy levels follow the analytical solution described in Sec. 3.1, which also exhibit some degree of degeneracy. In the regime where the interacting and tunneling terms are comparable the degeneracy is lifted, and there is an involved evolution of the spectrum where many avoided crossings appear. In this part, there is a heavy mixing of the basis states and, consequently, there is a strong change in the eigenstate structure. This intricate part of the spectrum is the region where one would expect a chaotic phase to emerge.

4.4 Numerical characterization of the chaotic phase

Once the basic spectral properties of the system have been discussed and the role of avoided crossings has been understood, one can proceed to characterize numerically the spectrum and eigenstates and assess the emergence of a chaotic phase. In order to do such characterization, a comparison of the energy spectrum against Random Matrix Theory is done by means of the level spacing ratio, as discussed in Sec. 2.3. In addition, the eigenstates structure is analyzed and connected to the emergence of the chaotic phase, for which the use of the quantity $\tilde{D}_1$ is needed, as mentioned in Sec. 2.3.

Two cases are analyzed. The first one consists in fixing a value of F/U, hence measuring the tilt in units of the interaction energy, and varying the relative tunneling strength J/U to see when chaos appears in the system and how it evolves for different tilt strength F/U

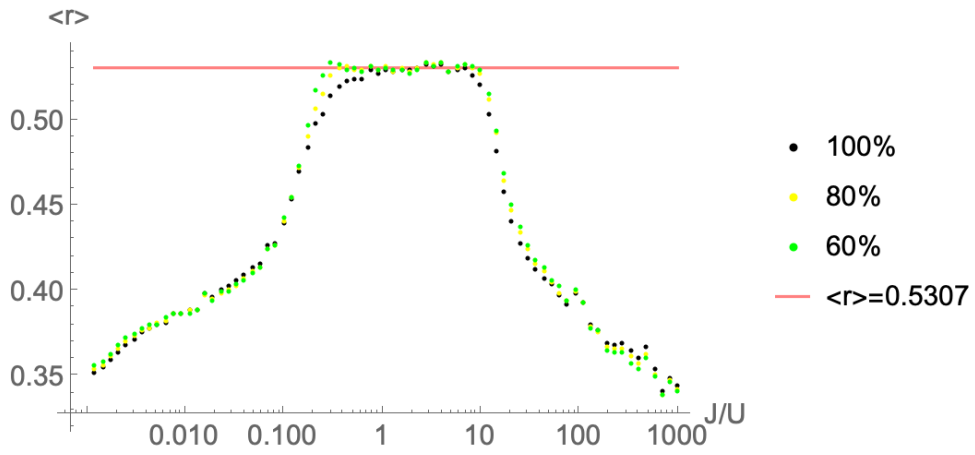

Figure 4.4: $\langle r \rangle$ with its uncertainties as a function of J/U considering different percentages of the inner energy spectrum, compared to $\langle r_{GOE} \rangle = 0.5307$, for the case $F = 0$ and $L = N = 10$.

values. In the second case, U/J is fixed and the tilt strength F/J, i.e., in units of the tunneling energy, is continuously varied.

4.4.1 Fixed value of F/U, varying J/U

First of all, the case $F/U = 0$ is analyzed. A Bose-Hubbard model formed by 10 bosons and 10 sites is simulated, whose dimension is dictated by Eq. (4.1), giving dim $H = 92378$. In this case, the values of J/U correspond to 75 equally spaced (in logarithmic scale) values, going from 0.001 to 831.75. It should be remarked that we remove the parity symmetry of the system, and hence work with an irreducible subspace of the Hilbert space.

As it was discussed in Sec. 2.3, in order to check the existence of chaos, one can calculate the mean value of the level spacing ratio r_n, defined in Eq. (2.29), and compare it against Random Matrix Theory. Equation (2.30) dictates that, when working with subspaces of the Hilbert space with no remaining symmetries, a value of $\langle r_{GOE} \rangle = 0.5307$ indicates the emergence of spectral chaos in the system.

In order to get an idea of the range of values of J/U where chaos appears in the absence of tilt $F = 0$, the mean value of the level spacing ratio for the whole spectrum for each value of J/U is calculated. The results obtained for the simulations appear in Fig. 4.4. It can be seen that that the region where chaos appears is that in which the value of J is roughly comparable to U. When taking only the 60% (removing the 20% higher and lower energy values) of the spectrum into account for the calculations, results show a clearer chaotic behaviour for a wider range of values of J/U, as it extends from $J/U \simeq 0.3$ to $J/U \simeq 8$. In the case of considering the 100% of the spectrum, the range is a little narrower, going approximately from $J/U \simeq 0.6$ to $J/U \simeq 6$. Considering the 80% of the spectrum (removing the 10% higher and lower energy values) results show an intermediate width, extending from $J/U \simeq 0.3$ to $J/U \simeq 7$.

In order to have a deeper understanding of the chaotic phase, it is convenient to obtain an energy resolved picture of such regime and do its characterization in terms of the eigenvector structure as well.

A Bose-Hubbard model with 9 bosons and 9 sites is considered in the following, first taking

$F/U = 0.01$. The dimension of the system is $\dim H = 24310$. It can be appreciated from Fig. 4.5(a) that the range of values for which chaos emerges is obviously similar to the case $F/U = 0$ and $L = N = 10$. The same behaviour can be deduced from Fig. 4.5(b), where the $\langle r \rangle$ values are calculated dividing the whole energy spectrum in a hundred equally spaced bins, and the calculations are done only for the states that fall into each of these bins. In this figure, one can see that the values J/U contained in the range $J/U \approx [0.1 - 10]$ show a difference $\langle r \rangle - 0.5307 \ll 1$. Thus, one can state that the zone in brighter color is the one that presents a chaotic behaviour. One can also see that within the mentioned region there is a dependence of quantum chaos on energy. For $J/U \simeq 0.1$, chaos is present in the lower parts of the ϵ spectrum, whereas for $J/U \sim 10$, chaos emerges in the highest half of the spectrum. In the middle, a chaotic behaviour can be observed for most of the ϵ values.

As presented in Sec. 2.3, the properties of the structure of the eigenstates can provide useful information about chaos. In Fig. 4.6(a), it can be seen that for the zone where the mean level spacing ratio plot indicated a chaotic behaviour of the system, the mean value of the first generalized fractal dimension (again, obtained by dividing the energy spectrum in equally spaced bins and calculating the mean value of $\tilde{D}_1$ for the states that fall into each bin) tends to one. As discussed in Sec. 2.3, this indicates that in this region the states become extended in the Fock basis. It can be observed that the strongly-interacting limit $J/U \ll 1$ shows a mean value of $\tilde{D}_1$ close to zero. On the contrary, the non-interacting limit $J/U \gg 1$ presents high values of $\tilde{D}_1$ slightly below those within the chaotic regime. Both cases can be understood if one thinks of the form of the Hamiltonian matrix. In the first limit, the matrix is diagonal in the on-site Fock state basis, which leads to heavily localized states. On the other hand, when taking the non-interacting limit, the off-diagonal terms become more relevant, leading to a delocalization of the states. These two situations were related in Sec. 2.3 to $\langle \tilde{D}_1 \rangle \to 0$ and $\langle \tilde{D}_1 \rangle \to 1$, respectively, matching with the results depicted in the plot.

One can analyze the width of the distribution of $\tilde{D}_1$ in a specific range of ϵ by calculating the variance over the corresponding eigenstates. Figure 4.6(b) depicts the variance of $\tilde{D}_1$. The same region in which Fig. 4.5(b) marks the emergence of chaos, i.e., $J/U \approx [0.1 - 10]$, shows now a strongly suppresed value of the variance of $\tilde{D}_1$. This supression indicates that all eigenstates close in energy share the same value of $\tilde{D}_1$, i.e., that all eigenstates close in energy exhibit the same structure.

As it was first shown in Refs. [22, 23, 24, 25], the analysis of $\tilde{D}_1$ and its mean and variance provide a very sensitive probe for the emergence of chaos.

Once we have understood how to identify the chaotic regime in the case $F/U = 0.01$, the evolution of the chaotic phase as the tilt strength is increased can be analyzed. In Fig. 4.7, the quantities $\langle r \rangle$, $\langle \tilde{D}_1 \rangle$ and $\mathrm{var}(\tilde{D}_1)$ as functions of J/U for eight selected values of F/U, ranging from $F/U = 0.01$ to $F/U = 100$, are shown. In Appendix A, the evolution for more values of F/U is presented.

It can be observed that the chaotic region changes smoothly when changing the tilt strength F/U, and tends to be displaced to the right while increasing J/U. This can be reasoned by the fact that increasing F/U gives the diagonal terms of the matrix a greater strength, the off-diagonal ones becoming less relevant. In other words, the states tend to be more localized. Hence, in order to increase the weight of the off-diagonal terms that could induce mixing of the basis states and hence the delocalization of the eigenstates required for the emergence of chaos, greater values of J/U are required, leading to a displacement of the chaotic phase to the right.

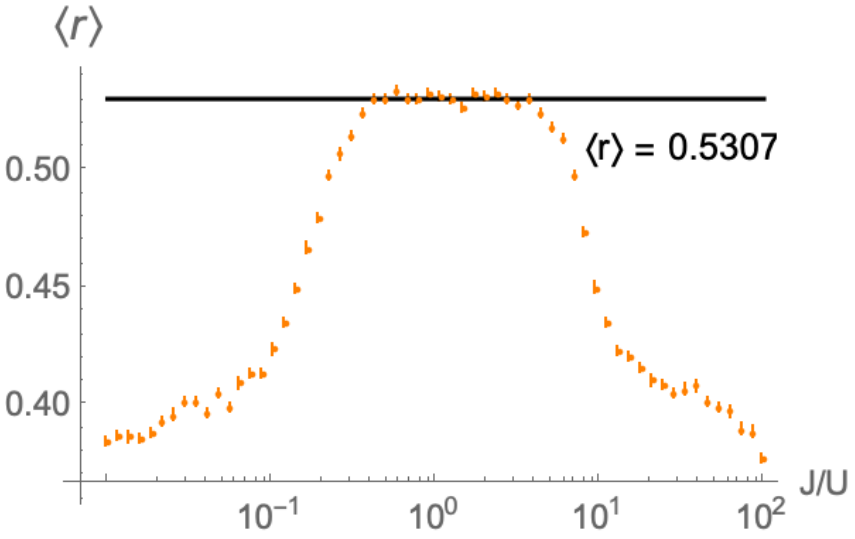

(4.5(a)) $\langle r \rangle$ with its uncertainties as a function of J/U avergaed over the whole energy spectrum, compared to $\langle r_{GOE} \rangle = 0.5307$.

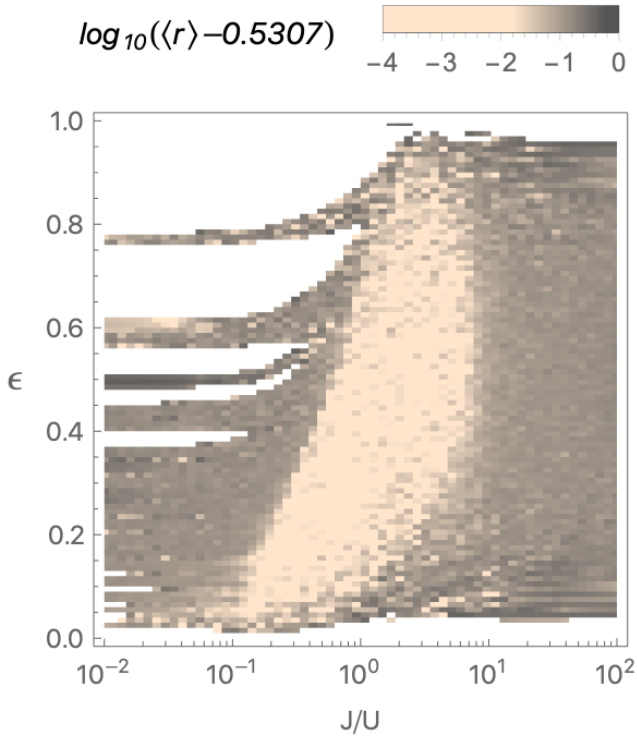

(4.5(b)) Mean level spacing ratio $\langle r \rangle$ versus J/U and scaled energy ϵ, compared to $\langle r_{GOE} \rangle = 0.5307$.

Figure 4.5: Mean level spacing ratio in a tilted Bose-Hubbard system with $L = N = 9$ and $F/U = 0.01$ compared against Random Matrix Theory.

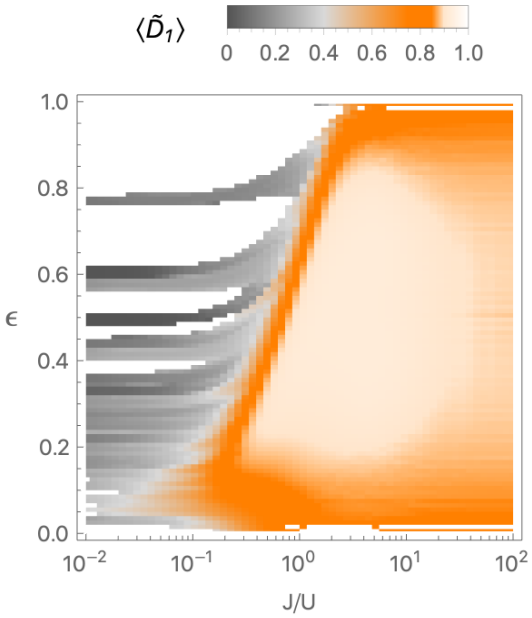

(4.6(a)) Mean value of the first generalized fractal dimension $\tilde{D}_1$.

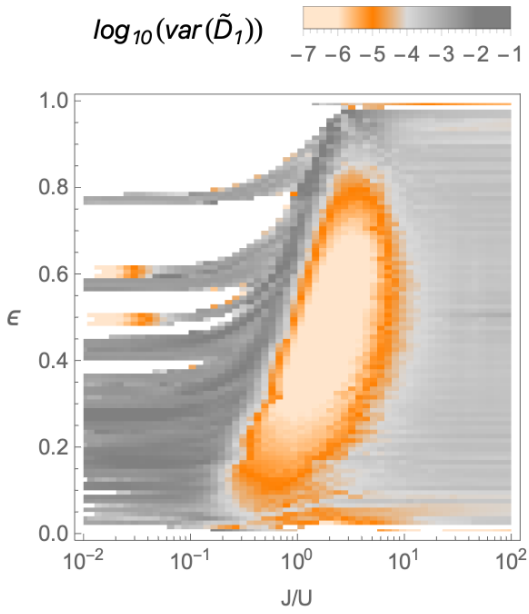

(4.6(b)) Variance of the first generalized fractal dimension $\tilde{D}_1$.

Figure 4.6: Examination of the eigenvector structure through fractal dimensions as a function of J/U and ϵ in the tilted Bose-Hubbard Hamiltonian for $N = L = 9$ and $F/U = 0.01$.

The chaotic phase disappears eventually for very large values of F/U, at least within the represented J/U range of values. As one approaches the limit where the tilt term is dominant, i.e., $F/U \gg 1$, one would expect not to see a chaotic behaviour, as this limit corresponds to the analytical case studied in Sec. 3.3 which does not present any chaotic behaviour.

One could wonder for which values of F/U the chaotic region disappears and the ones for which the chaotic region is wider. In order to find these F/U values, one may use the energy-averaged $\langle r \rangle$ and study its deviation from $\langle r_{GOE} \rangle$ up to a given *tolerance*. Then, for each F/U one can locate the lowest value of J/U for which such deviation is lower or equal than this tolerance, as well as the highest one, obtaining the range of values of J/U that exhibit chaos. In Fig. 4.8(a) the results for three different tolerances are shown. It can be observed that the maximum J/U value exhibiting chaos grows with the tilt strength, until it reaches a maximum and then decreases. The minimum J/U value remains almost constant with F/U, showing a slight increase for great values of F/U.

Particularly, considering a 0.5% tolerance, the widest range of J/U values for which the system is considered to be chaotic appears at $F/U = 0.599484$. Considering a 1% tolerance, such range appears at $F/U = 0.774263$. For the 2% tolerance case, the widest range occurs at $F/U = 1$. Thus, the system exhibits a more chaotic behavior in the case where the three parameters J, F, and U are similar.

4.4.2 Fixed value of U/J, varying F/J

An analogous study is done by setting a value of U/J and analyzing the evolution of the system when the tilt strength measured in units of the tunneling energy is continuously

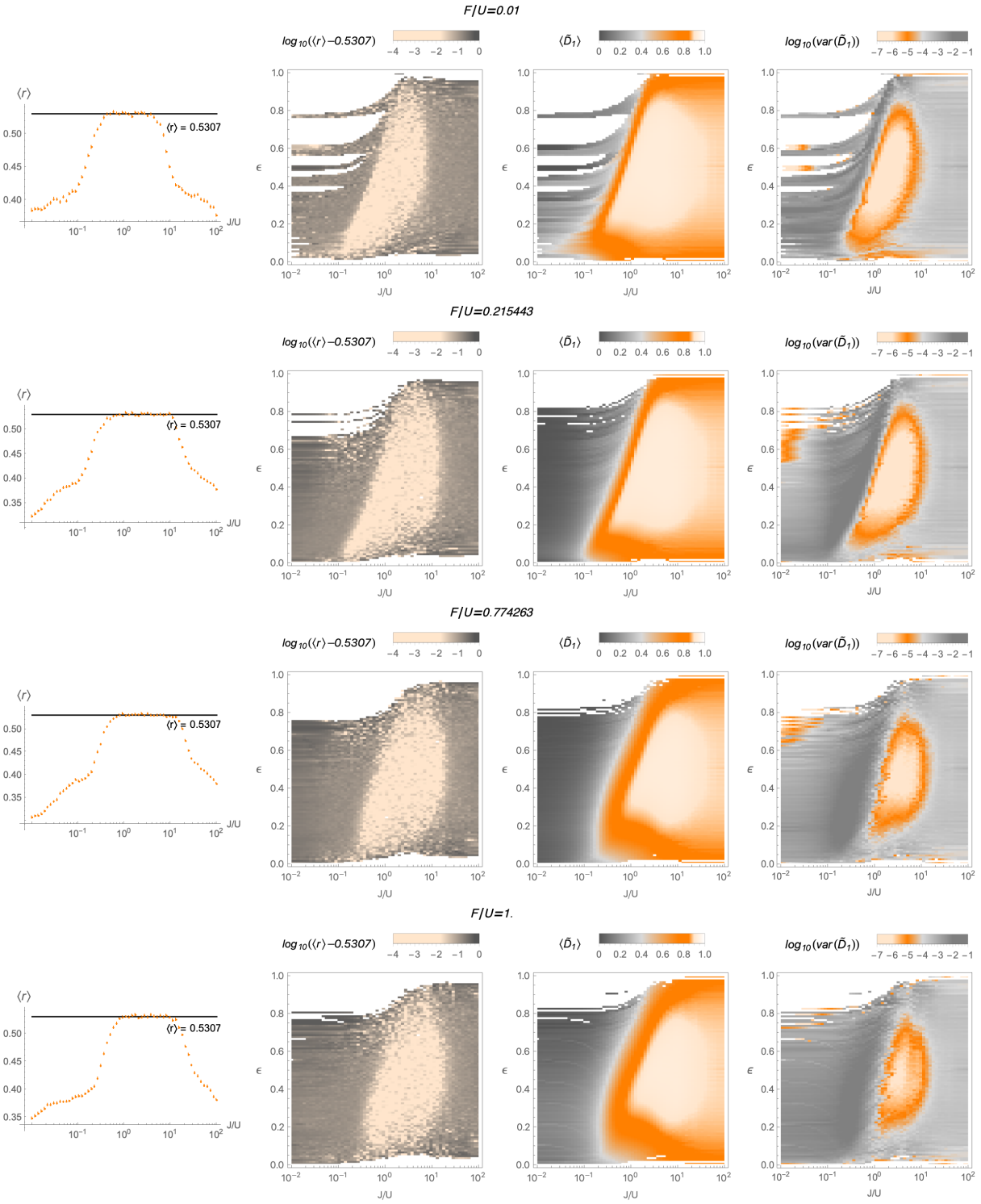

Figure 4.7: Spectral and eigenvector properties of the tilted Bose-Hubbard Hamiltonian as functions of J/U for different values of F/U (increasing from top to bottom). The shown figures of merit are (from left to right), energy-averaged $\langle r \rangle$ (over full spectrum), energy-resolved difference $\langle r \rangle - \langle r_{GOE} \rangle$, mean value of first generalized fractal dimension and variance of first generalized fractal dimension.

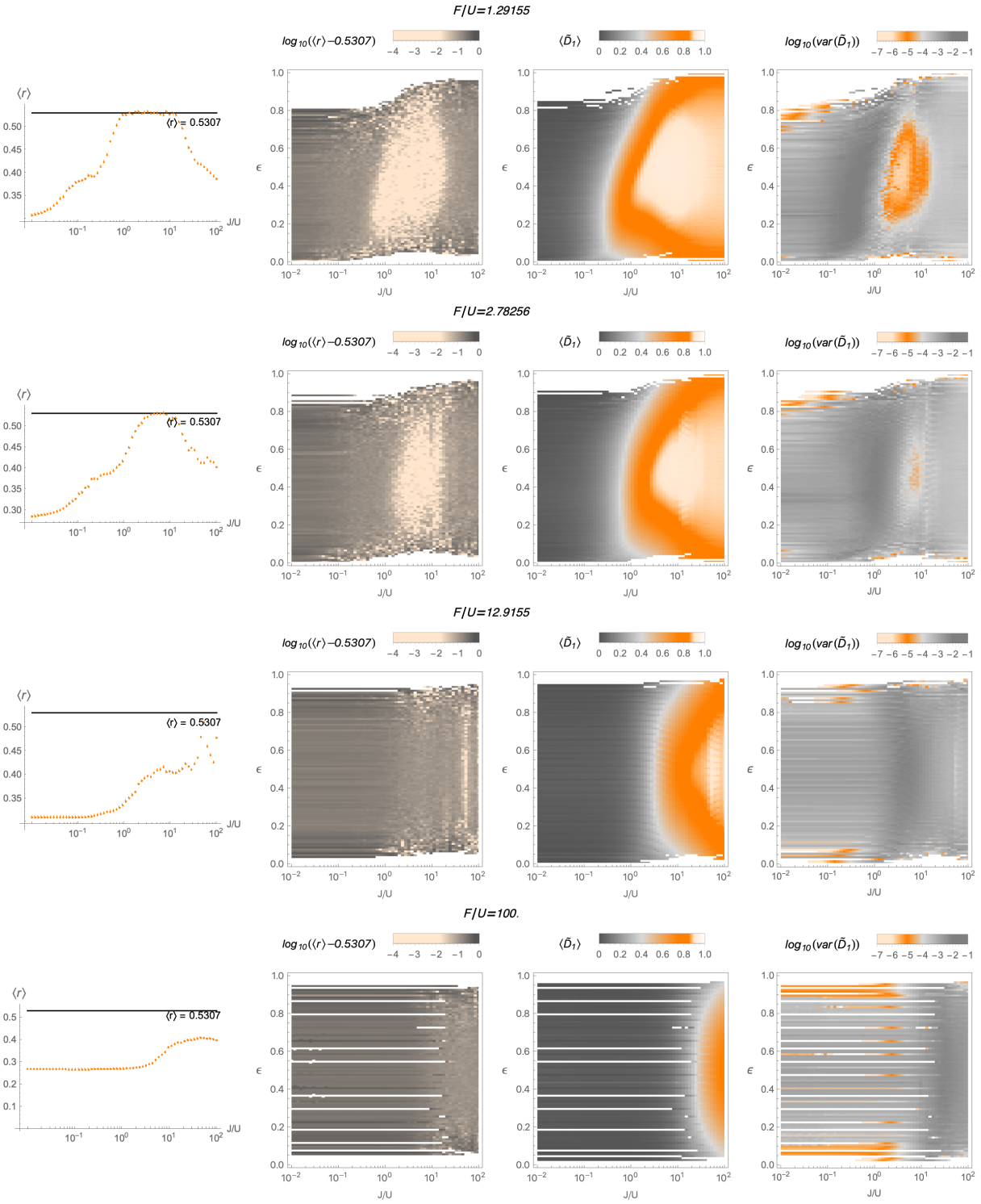

Figure 4.7: Spectral and eigenvector properties of the tilted Bose-Hubbard Hamiltonian as functions of J/U for different values of F/U (increasing from top to bottom). The shown figures of merit are (from left to right), energy-averaged $\langle r \rangle$ (over full spectrum), energy-resolved difference $\langle r \rangle - \langle r_{GOE} \rangle$, mean value of first generalized fractal dimension and variance of first generalized fractal dimension.

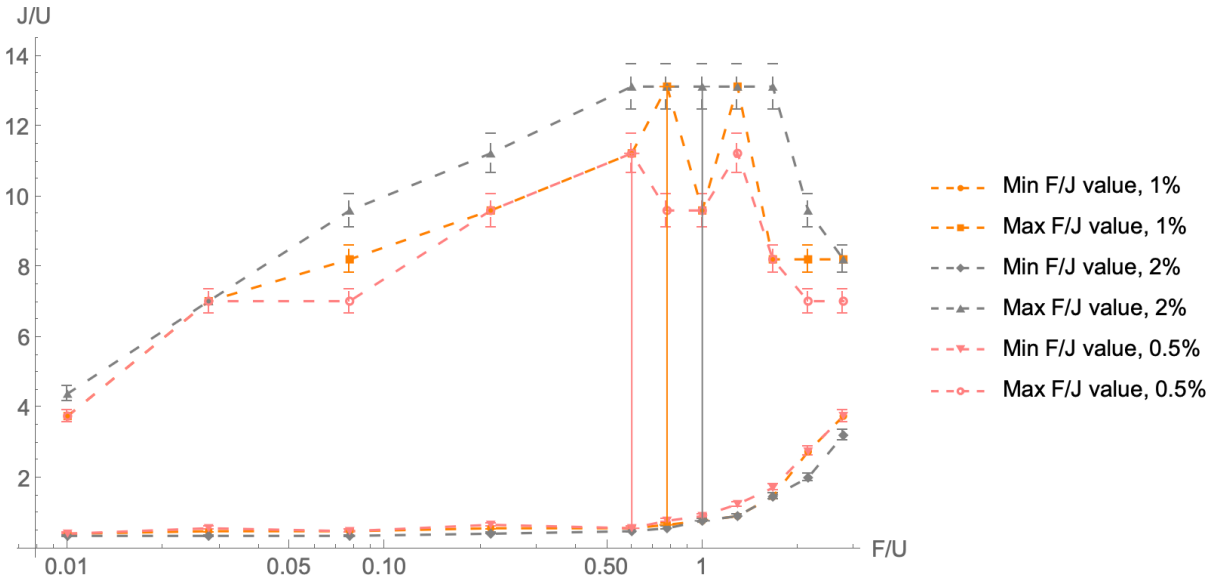

(4.8(a)) Maximum and minimum values of J/U as functions of F/U for which the system is considered to be in the chaotic region according to the comparison of the energy-averaged $\langle r \rangle$ and $\langle r_{GOE} \rangle$, for different tolerances. The bars mark the maximum width of the chaotic region for each tolerance.

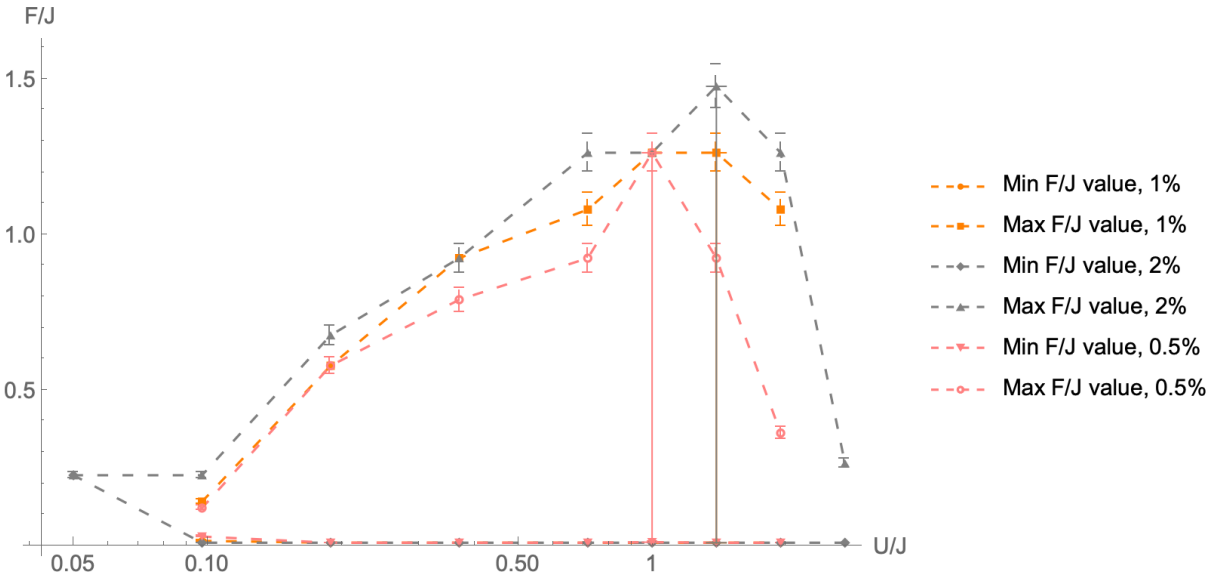

(4.8(b)) Maximum and minimum values of F/J as functions of U/J for which the system is considered to be in the chaotic region according to the comparison of the energy-averaged $\langle r \rangle$ and $\langle r_{GOE} \rangle$, for different tolerances. The bars mark the maximum width of the chaotic region for each tolerance.

Figure 4.8: Analysis of the width of the chaotic phase in the system for the case $L = N = 9$ (see Figs. 4.7, 4.9, A.1 and A.2).

increased , using again a model formed by 9 bosons and 9 sites. In this case, Fig. 4.9 shows the evolution of quantum chaos for several discrete values of U/J going from $U/J = 0.05$ to $U/J = 20$. Only eight selected U/J values are presented in Fig. 4.9, the rest of them are shown in Appendix A.2.

It can be observed that for weak interaction ($U/J = 0.05$), as expected, there is no fully developed chaotic phase. Although, the mean of $\tilde{D}_1$ shows a region which indicates of the states, due to the dominance of the tunneling term. Only a weak trace of spectral chaos appears in the spectrum. As soon as $U/J \gtrsim 0.1$, a chaotic phase emerges over the region $F/J \approx [0.01 - 1]$, beyond which it ends abruptly. In the tilted-dominated limit $F/J \gg 1$ the system approaches the analytical case studied in Sec. 3.2, for which no chaotic phase emerges.

As U/J increases, the chaotic phase initially persists, and in fact it seems to extent slightly towards higher F/J values, but exhibiting a sharp end in all cases. The chaotic phase for weak interaction strength values covers almost the entire energy spectrum, but its energy span starts to shrink for $U/J \gtrsim 2$. This can be clearly observed in $\langle r \rangle$ as well as in the variance of $\tilde{D}_1$. As mentioned earlier, in the region where Random Matrix Theory predicts a specially chaotic behaviour, the variance of $\tilde{D}_1$ indicates that the eigenstates corresponding to close energies share the same delocalized structure.

As it was done in the previous section, the width of the chaotic phase is studied by monitoring the deviation of the energy averaged level spacing ratio from GOE prediction. The results for different chosen tolerances are depicted in Fig. 4.8(b). It is noticeable that the maximum F/J values for which chaos can be observed grow almost linearly with U/J, and then drop abruptly. The minimum F/J values remain close to zero independently of U/J. Specifically, it can be observed that, considering a 0.5% tolerance, the widest chaotic range occurs at $U/J = 1$. Using a 2% tolerance, it appears at $U/J = 1.39495$. Lastly, the widest range of F/J values for which the system is considered to be chaotic using a 1% tolerance appears at $U/J = 1.39495$. Then, the system seems to present a more chaotic behavior when the three parameters J, F, and U are similar, in accordance with the results presented in the previous section.

4.4.3 Trajectory of the $|1, 1, ..., 1\rangle$ state

Many experiments carried out with cold atoms to probe the existence of quantum chaos are based on studying the dynamical evolution of an initial state. Such state is normally a Fock state in the on-site basis, and typically the lattice is initialized with a single atom per site, i.e., the chosen initial state is often the $|1, 1, ..., 1\rangle$ state [16, 26].

This experimental interest makes the study of the trajectory of the chosen Fock state as a function of the system parameters a relevant matter, as it can serve to assess how the state traverses the chaotic phase. Therefore, such study can be useful to determine the parametric region where chaos could be observed experimentally when employing such Fock state.

Figures 4.10(a) and 4.10(b) show how the Fock state with homogeneous density evolves in the parametric spaces $(\epsilon, J/U)$ and $(\epsilon, F/J)$, respectively, and gets into the chaotic phase of the system. In red, the energy trajectory of the state is represented while green lines mark the associated energy width ΔE,

$$(\Delta E)^2 = \langle H^2 \rangle - \langle H \rangle^2. \tag{4.19}$$

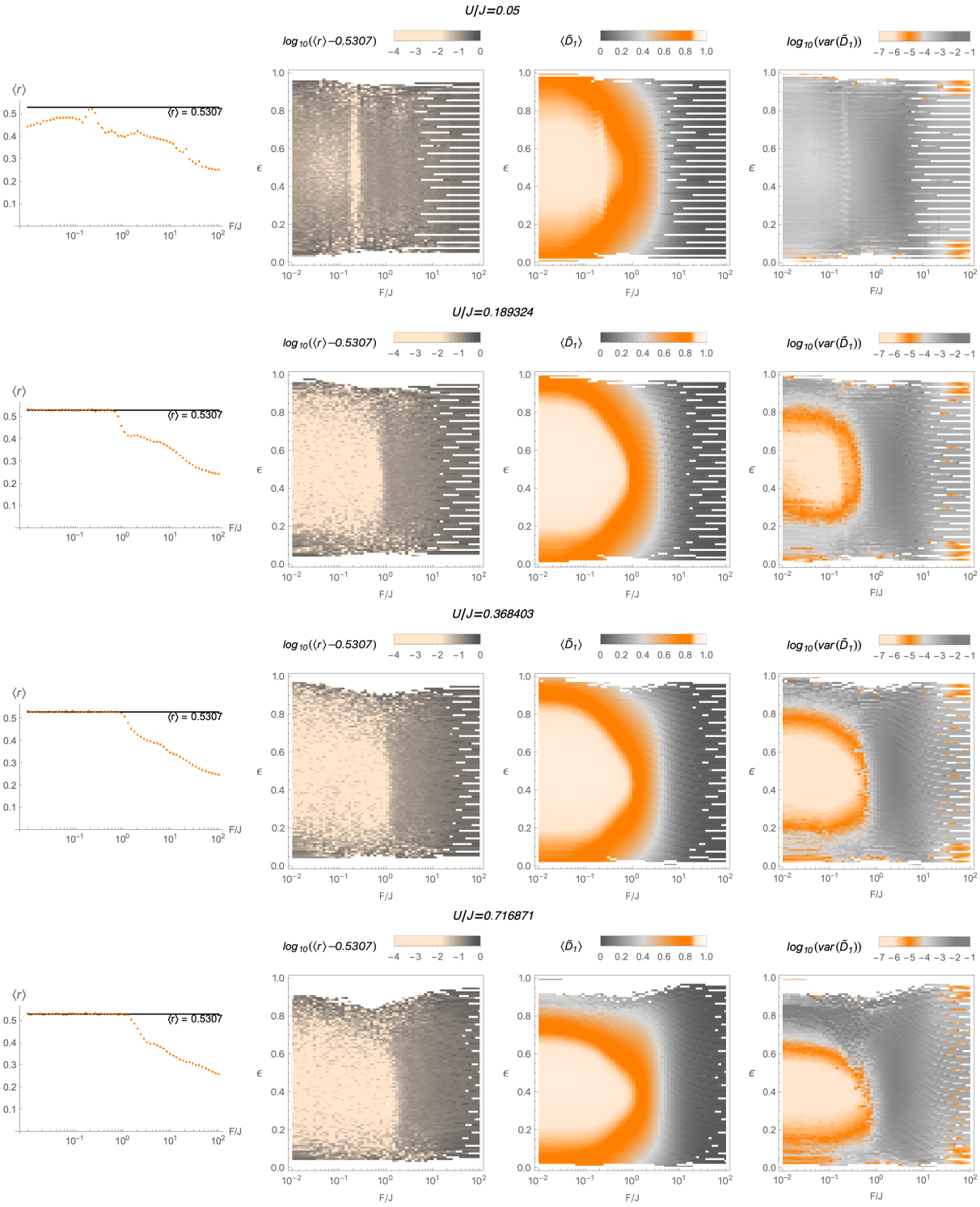

Figure 4.9: Spectral and eigenvector properties of the tilted Bose-Hubbard Hamiltonian as functions of F/J for different values of U/J (increasing from top to bottom). The shown figures of merit are (from left to right), energy-averaged $\langle r \rangle$ (over full spectrum), energy-resolved difference $\langle r \rangle - \langle r_{GOE} \rangle$, mean value of first generalized fractal dimension and variance of first generalized fractal dimension.

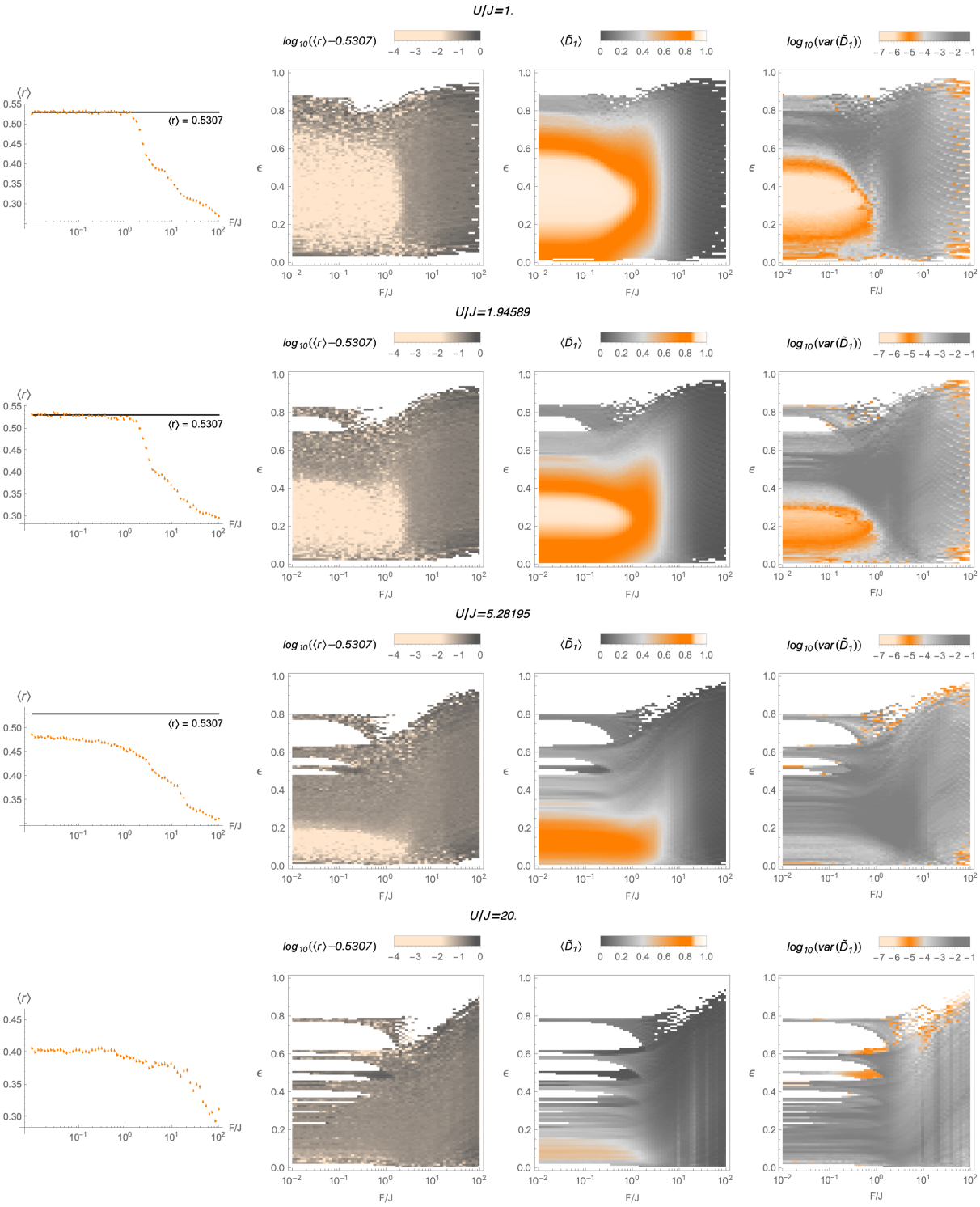

Figure 4.9: Spectral and eigenvector properties of the tilted Bose-Hubbard Hamiltonian as functions of F/J for different values of U/J (increasing from top to bottom). The shown figures of merit are (from left to right), energy-averaged $\langle r \rangle$ (over full spectrum), energy-resolved difference $\langle r \rangle - \langle r_{GOE} \rangle$, mean value of first generalized fractal dimension and variance of first generalized fractal dimension.

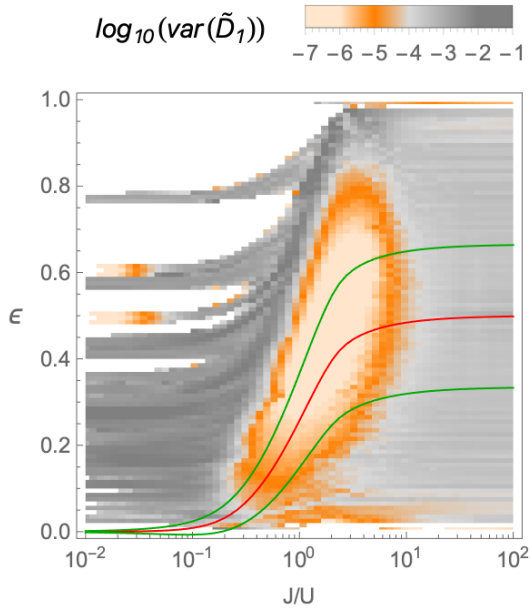

(4.10(a)) Evolution of the $|1, 1, \ldots, 1\rangle$ state with J/U for $F/U = 0.01$.

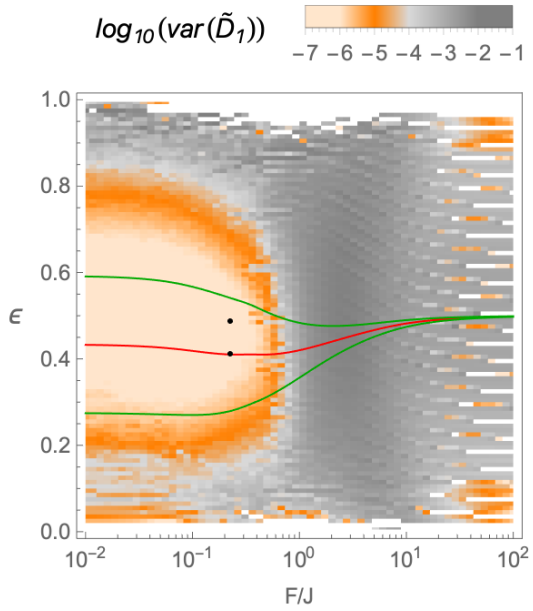

(4.10(b)) Evolution of the $|1, 1, \ldots, 1\rangle$ state with F/J for $U/J = 0.368403$. Symbols mark the ϵ values used for the analysis of Fig. 4.11.

Figure 4.10: Evolution of the $|1, 1, \ldots, 1\rangle$ state in the parametric spaces (a) $(\epsilon, J/U)$ and (b) $(\epsilon, F/J)$. The red lines indicate the energy trajectory and green lines mark the energy width ($\pm\Delta E$ of the state.)

It can be easily checked that $\langle H\rangle = 0$ for the $|1, 1, ..., 1\rangle$ state. The evaluation of $\langle H^2\rangle$ yields (see Appendix B)

$$\langle H^2\rangle = 4J^2(N-1). \tag{4.20}$$

Then,

$$\Delta E = 2J\sqrt{N-1}. \tag{4.21}$$

The energy width of the state is a magnitude of interest, since it provides information about the range of energies (and hence eigenstates) that participate noticeably in the eigenbasis expansion of the Fock state and, consequently, in its dynamics.

Figure 4.10(a) show that, for the case $F/U = 0.01$, the state enters the chaotic region from the lowest part of the spectrum, and remains within the chaotic phase for $J/U \approx [0.05 - 10]$. One can also see that in terms of the rescaled energy ϵ, $\Delta\epsilon$ is 0 in the non-interacting limit $J/U \ll 1$, and it starts to grow as the state gets into the chaotic regime. There, one has that a large portion of the eigenstates contained in the chaotic phase participate in the dynamics of the Fock state. When exiting the chaotic phase, this energy window remains wide, since as the non-interacting limit is approached a considerable range of eigenstates overlap with the $|1, 1, ..., 1\rangle$ state.

For the case $U/J = 0.368403$, the ϵ trajectory of the Fock state remains in the middle part of the spectrum for all F/J, and it is within the chaotic regime up to $F/J \approx 1$. Below this tilt strength, the majority of eigenstates that participate in the Fock state dynamics lies within the chaotic region, where ΔE covers more than a half of the chaotic domain. Almost as soon as the state exits the chaotic phase, such window narrows and drops rapidly to zero.

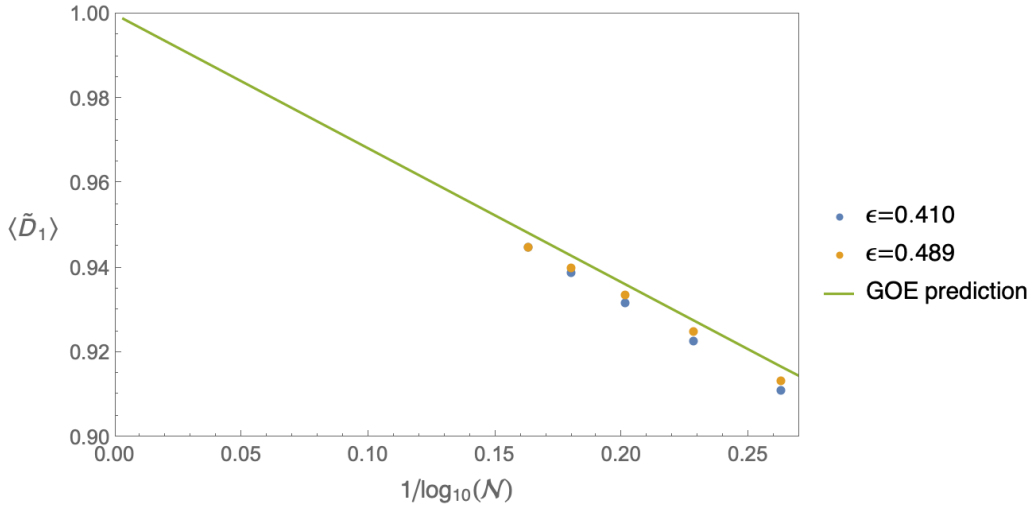

(4.11(a)) Mean value of the first generalized fractal dimension as a function of Hilbert space dimension, compared against GOE prediction.

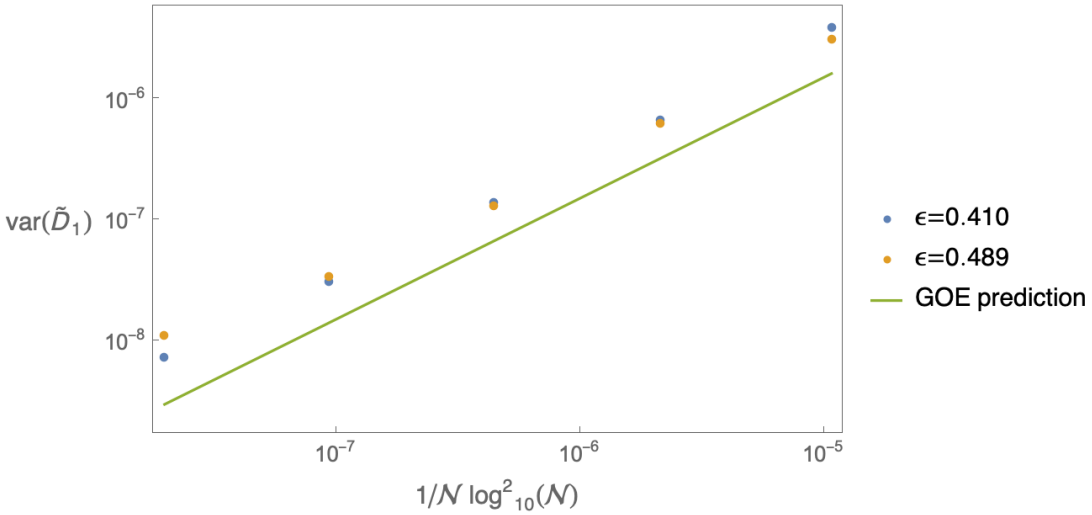

(4.11(b)) Variance of the first generalized fractal dimension as a function of Hilbert space dimension $\mathcal{N}$, compared against GOE prediction.

Figure 4.11: Evolution of the mean value and variance of the first generalized fractal dimension with the size of Hilbert space for $F/J = 0.22695$, $U/J = 0.368403$ and rescaled energies $\epsilon = 0.410$ and $\epsilon = 0.489$.

Finally, we may study the dependence of the eigenstate structure within the chaotic phase on the size of Hilbert space. We do this analysis in a region relevant for the dynamics of the homogeneous Fock state. We fix $U/J = 0.368403$ and $F/J = 0.22695$ and select the two rescaled energies $\epsilon = 0.410$ and $\epsilon = 0.489$, as indicated in Fig. 4.10(b).

We calculate the 500 eigenstates closest to those energy values for $L \in [8, 12]$ with Hilbert space sizes $\mathcal{N} \in [6435, 1351078]$ (see Tab. 4.1 on page 21) and obtain $\langle \tilde{D}_1 \rangle$ and $\mathrm{var}(\tilde{D}_1)$, which are compared against Random Matrix Theory predictions, that state [25]

$$\langle \tilde{D}_1 \rangle = 1 - \frac{1}{\ln \mathcal{N}} \left[2 - \gamma - \ln 2 - \frac{1}{\mathcal{N}} + O(\mathcal{N}^{-2}) \right], \tag{4.22}$$

where $\mathcal{N}$ is the dimension of Hilbert space, $\dim H$ and γ is Euler-Mascheroni constant [22]. Moreover

$$\mathrm{var}(\tilde{D}_1) = \frac{1}{\ln^2 \mathcal{N}} \left[\frac{3\pi^2 - 28}{2\mathcal{N}} + O(\mathcal{N}^{-2}) \right]. \tag{4.23}$$

The results for our simulation are shown in Fig. 4.11. Despite the quantitative deviations, we see that as the thermodynamical limit is approached, Fig. 4.11(a) shows that $\langle \tilde{D}_1 \rangle \to 1$, and Fig. 4.11(b) probes that $\mathrm{var}(\tilde{D}_1) \to 0$, both quantities exhibiting the functional dependence on $\mathcal{N}$ predicted by Random Matrix Theory.

5 | Conclusions

During this thesis several aspects of the Bose-Hubbard model have been studied. In the first place, the cases that admit analytical solutions have been presented and were used to describe qualitatively the ground state phase transition between a superfluid to a Mott insulator that occurs as a function of the ratio between the tunneling energy J and the interaction energy U.

Later, the features of the model for small number of bosons and sites were analyzed, studying the evolution of the energy levels as functions of J/U and of the tilt strength F/U. We observed the emergence of level repulsion in the spectrum induced by the off-diagonal couplings in the Hamiltonian due to the tunneling term. Hence, real crossings at $J/U \to 0$ become avoided crossings when increasing the tunneling term. Moreover, we discussed that avoided crossings change the eigenstates structure, and induce a strong mixing in the considered basis.

Then, we considered larger systems to characterize the chaotic phase and its evolution with the parameters of the Hamiltonian. Firstly, we observed such evolution with J/U after fixing the value of F/U, and simulations showed that the chaotic phase emerged in the regions were the three parameters were similar. The chaotic region was identified from the agreement of spectral statistics with Random Matrix Theory, and we observed that it was characterized by delocalized eigenstates that share the same structure in Fock space.

Different fixed values of F/U were used, showing that there is a range of F/U values for which the chaotic range width maximizes. An analogous study was done by fixing U/J and varying F/J. Moreover, the structure of the eigenstates was particularly useful to indicate the emergence of chaos. We found that chaos is maximized typically when the tunneling energy, the interaction strength and the tilt parameter are comparable. Although, as a function of F/J the chaotic phase was seen to end sharply with $F/J > 1$, an interesting feature to be investigated in further studies.

The trajectories of the homogeneous Fock state with unit density in the parametric space of the system were simulated in order to understand how such state sees the chaotic phase as a function of J/U or F/J. For very weak tilt ($F/U = 0.01$), the Fock state traverses the chaotic phase in the range $J/U \simeq [0.05 - 10]$. In the presence of both tilt and interaction, for $U/J = 0.368403$, the Fock state energy trajectory remains within the chaotic domain for $F/J \simeq [0 - 1]$. In both cases, the energy width shows that the dynamics of the homogeneous Fock state is mostly determined by eigenstates in the chaotic phase.

Finally, we analyze the evolution of the mean value and variance of the first generalized fractal dimension with the dimension of Hilbert space, and compare the results with Random Matrix Theory predictions. Results showed accordance with the functional dependence dictated by Random Matrix Theory for both cases.

6 | Conclusiones

A lo largo del trabajo se han estudiado diversos aspectos relativos al modelo de Bose-Hubbard. En primer lugar, se desarrollan los tres límites con solución analítica del modelo, y se utilizan para describir cualitativamente la transición de fase que tiene lugar en el estado fundamental desde un estado superfluido a un estado de aislante de Mott, que ocurre en función del valor que tome la energía de *tunneling* con respecto a la de interacción.

Posteriormente, se analizan las características del modelo utilizando un número pequeño de bosones y sitios, estudiando la evolución de los niveles energéticos del sistema como función de la relación J/U y de la intensidad del campo externo F/U. Observamos la aparición de repulsión de niveles el espectro energético provocada por los términos no diagonales del Hamiltoniano, que aparecen a causa de la presencia del término de *tunneling*. Así, los cruces reales en el límite $J/U \to 0$ se convierten en niveles repelidos al aumentar el término de *tunneling*. Además, discutimos el hecho de que la repulsión de niveles cambia la estructura de los autoestados, dando lugar a una mezcla de los mismos en la base considerada.

Consideramos sistemas de dimensión mayor y caracterizamos la fase caótica a través del estudio de la evolución de la misma como función de los parámetros del Hamiltoniano. Primero, observamos dicha evolución en función de J/U, habiendo fijado previamente el valor de F/U, viendo que nuestras simulaciones demuestran que la fase caótica aparece para aquellas regiones en que los tres parámetros del Hamiltoniano son del mismo orden. La región de la fase caótica se identifica a través de las predicciones sobre el espectro energético dadas por la Teoría de Matrices Aleatorias.

Se han usado diversos valores de F/U, mostrando así que existe un rango de valores para el cual el ancho de la fase caótica se maximiza. Se ha llevado a cabo un estudio análogo fijando el valor de U/J y variando F/J. Además, la estructura de los autoestados ha sido particularmente útil a la hora de indicar la presencia de caos. De hecho, encontramos que el caos se maximiza típicamente en aquellas regiones en que la energía de *tunneling*, la fuerza de interacción y la intensidad del campo externo son de orden similar.

Sin embargo, se comprueba que la fase caótica termina abruptamente al evolucionar con F/J cuando se alcanzan valores $F/J > 1$, lo cual supone una característica que puede resultar interesante para estudios futuros.

La trayectoria del estado de Fock homogéneo con densidad unidad en el espacio paramétrico del sistema ha sido simulada con el objetivo de entender cómo dicho estado ve la fase caótica en función tanto de J/U como de F/J. En el caso de campos muy débiles (F/U=0.01), el estado de Fock atraviesa la fase caótica en el rango $J/U \simeq [0.05 - 10]$. En presencia de campo y de término de interacción, para un valor $U/J = 0.368403$, la trayectoria del estado de Fock se mantiene dentro del dominio de la fase caótica para

$F/J \simeq [0-1]$. En ambos casos, el ancho de energías muestra que la dinámica del estado de Fock homogéneo viene fundamentalmente determinada por los autoestados pertenecientes a la fase caótica.

Por último, analizamos la evolución del valor medio y la varianza de la primera dimensión fractal generalizada con la dimensión del espacio de Hilbert, y comparamos los resultados con la predicción teórica de la Teoría de Matrices Aleatorias. Los resultados muestran acuerdo con la dependencia predicha por la Teoría de Matrices Aleatorias.

Bibliography

[1] B. P. Anderson and M. A. Kasevich. Macroscopic quantum interference from atomic tunnel arrays. *Science*, 282:1686–1689, 11 1998.

[2] Immanuel Bloch, Jean Dalibard, and Sylvain Nascimbène. Quantum simulations with ultracold quantum gases. *Nature Physics*, 8:267–276, 2012.

[3] Andreas Buchleitner and Andrey R. Kolovsky. Interaction-Induced Decoherence of Atomic Bloch Oscillations. *Physical Review Letters*, 91:253002, 2003.

[4] Piers Coleman. *Introduction to Many Body Physics*. Cambridge University Press, 2015.

[5] Matthew P. A. Fisher, Peter B. Weichman, G. Grinstein, and Daniel S. Fisher. Boson localization and the superfluid-insulator transition. *Physical Review B*, 40:546–570, 1989.

[6] Zachary A. Geiger, Kurt M. Fujiwara, Kevin Singh, Ruwan Senaratne, Shankari V. Rajagopal, Mikhail Lipatov, Toshihiko Shimasaki, Rodislav Driben, Vladimir V. Konotop, Torsten Meier, and David M. Weld. Observation and Uses of Position-Space Bloch Oscillations in an Ultracold Gas. *Physical Review Letters*, 120:213201, 5 2018.

[7] Olivier Giraud, Nicolas Macé, Éric Vernier, and Fabien Alet. Probing symmetries of quantum many-body systems through gap ratio statistics. *Phys. Rev. X*, 12:011006, 2022.

[8] Markus Greiner and Simon Fölling. Condensed-matter physics: optical lattices. *Nature*, 453:736–738, 2008.

[9] Markus Greiner, Olaf Mandel, Tilman Esslinger, Theodor W Hänsch, and Immanuel Bloch. Quantum phase transition from a superfluid to a Mott insulator in a gas of ultracold atoms. *Nature*, 415(6867):39–44, 2002.

[10] C. Gross and W.S. Bakr. Quantum gas microscopy for single atom and spin detection. *Nature Physics*, 17:1316, 2021.

[11] Christian Gross and Immanuel Bloch. Quantum simulations with ultracold atoms in optical lattices. *Science*, 357:995–1001, 2017.

[12] Fritz Haake, Sven Gnutzmann, and Marek Kuś. *Quantum Signatures of Chaos*. Springer International Publishing, fourth edition, 2018.

[13] Elmar Haller, Russell Hart, Manfred J. Mark, Johann G. Danzl, Lukas Reichsöllner, and Hanns-Christoph Nägerl. Inducing Transport in a Dissipation-Free Lattice with Super Bloch Oscillations. *Physical Review Letters*, 104:200403, 5 2010.

[14] T Hartmann, F Keck, H J Korsch, and S Mossmann. Dynamics of Bloch oscillations. *New Journal of Physics*, 6(1):2, 2004.

[15] D. Jaksch, C. Bruder, J. I. Cirac, C. W. Gardiner, and P. Zoller. Cold bosonic atoms in optical lattices. *Phys. Rev. Lett.*, 81:3108–3111, 1998.

[16] Adam M Kaufman, M Eric Tai, Alexander Lukin, Matthew Rispoli, Robert Schittko, Philipp M Preiss, and Markus Greiner. Quantum thermalization through entanglement in an isolated many-body system. *Science*, 353:794–800, 2016.

[17] A. R Kolovsky and A Buchleitner. Quantum chaos in the Bose-Hubbard model. *Europhysics Letters (EPL)*, 68(5):632–638, 2004.

[18] Andrey R. Kolovsky and Hans Jürgen Korsch. Bloch oscillations of cold atoms in optical lattices. *International Journal of Modern Physics B*, 18:1235–1260, 2004.

[19] Konstantin V. Krutitsky. Ultracold bosons with short-range interaction in regular optical lattices. *Physics Reports*, 607:1–101, 2016.

[20] Jakob Lindinger. Multifractal properties of the ground state of the Bose-Hubbard model. MSc Thesis. Albert-Ludwigs-Universität Freiburg. 2017.

[21] Edward Ott. *Chaos in dynamical systems*. Cambridge University Press, 1993.

[22] Lukas Pausch. Eigenstate structure and quantum chaos in the Bose-Hubbard Hamiltonian. PhD Thesis. Albert-Ludwigs-Universität Freiburg. 2022.

[23] Lukas Pausch, Andreas Buchleitner, Edoardo G. Carnio, and Alberto Rodríguez. Optimal route to quantum chaos in the Bose–Hubbard model. *Journal of Physics A: Mathematical and Theoretical*, 55:324002, 2022.

[24] Lukas Pausch, Edoardo G. Carnio, Andreas Buchleitner, and Alberto Rodríguez. Chaos in the Bose-Hubbard model and Random Two-Body Hamiltonians. *New Journal of Physics*, 23:123036, 2021.

[25] Lukas Pausch, Edoardo G. Carnio, Alberto Rodríguez, and Andreas Buchleitner. Chaos and ergodicity across the energy spectrum of interacting bosons. *Physical Review Letters*, 126:150601, 2021.

[26] Matthew Rispoli, Alexander Lukin, Robert Schittko, Sooshin Kim, M. Eric Tai, Julian Léonard, and Markus Greiner. Quantum critical behaviour at the many-body localization transition. *Nature*, 573:385–389, 2019.

[27] M. Schneider, A. Rodríguez, and A. Buchleitner. Fock space localization of many-body states in the tilted bose-hubbard model. *Acta Physica Polonica A*, 136:834–840, 2019.

[28] Marianne T. V. Schneider. Fock Space Localization of Many-Body States in the Tilted Bose-Hubbard Model. BSc Thesis. Albert-Ludwigs-Universität Freiburg. 2019.

[29] Thilo Stöferle, Henning Moritz, Christian Schori, Michael Köhl, and Tilman Esslinger. Transition from a Strongly Interacting 1D Superfluid to a Mott Insulator. *Physical Review Letters*, 92:130403, 2004.

A | Spectral and eigenvector properties of the Bose-Hubbard Hamiltonian

In this Appendix we present the results obtained for the simulations that show the spectral and eigenvector properties of the Bose-Hubbard Hamiltonian as functions of the Hamiltonian parameters.

A.1 Fixed value of F/U, varying J/U

The whole collection of figures obtained by the numerical simulations are shown in Fig. A.1.

A.2 Fixed value of U/J, varying F/J

In this part of the Appendix the results for the whole set of simulations of the evolution of chaos with U/J is shown, and can be seen in Fig. A.2.

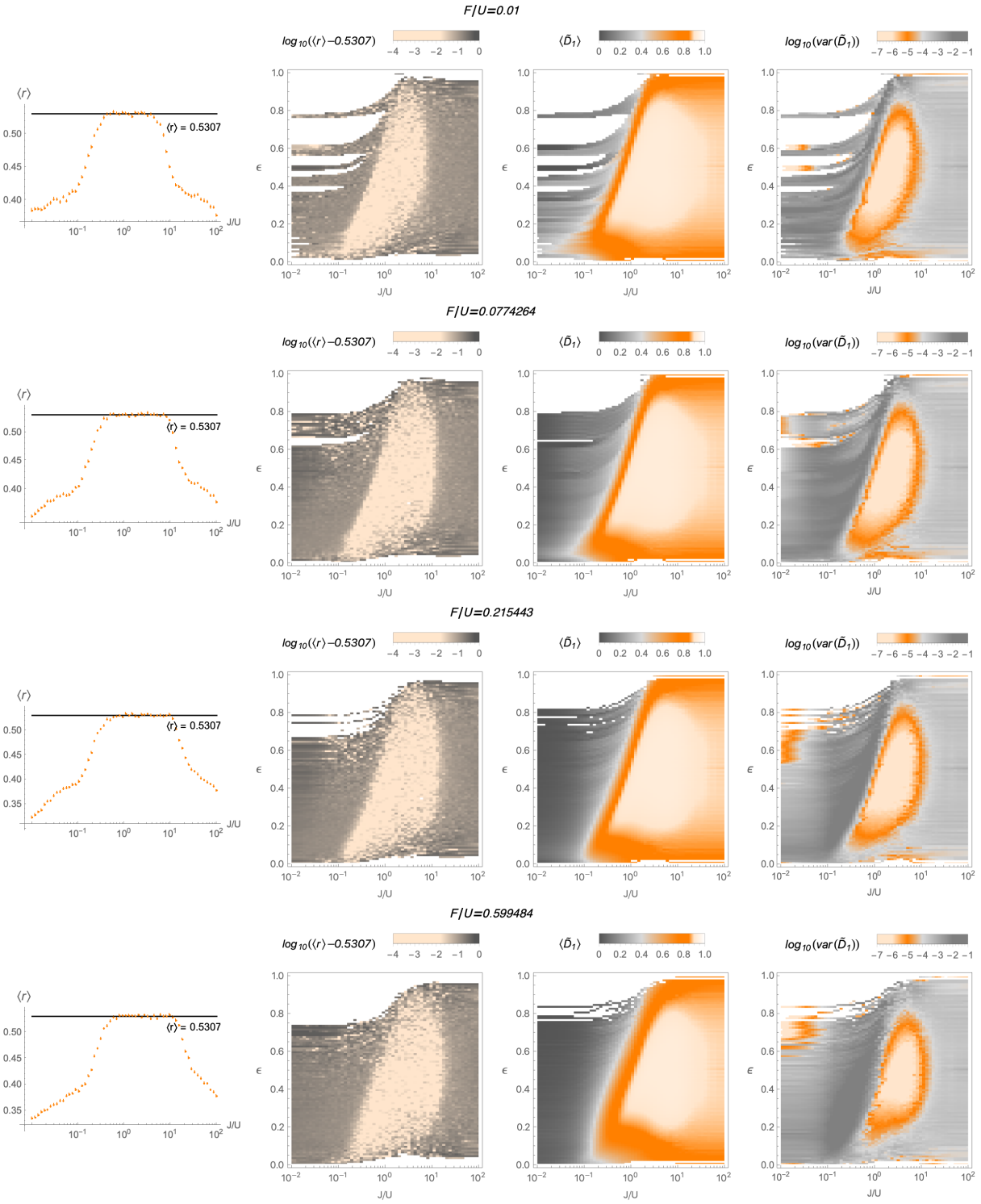

Figure A.1: Spectral and eigenvector properties of the tilted Bose-Hubbard Hamiltonian as functions of J/U for different values of F/U (increasing from top to bottom). The shown figures of merit are (from left to right), energy-averaged $\langle r \rangle$, energy-resolved difference $\langle r \rangle - \langle r_{GOE} \rangle$, mean value of first generalized fractal dimension and variance of first generalized fractal dimension.

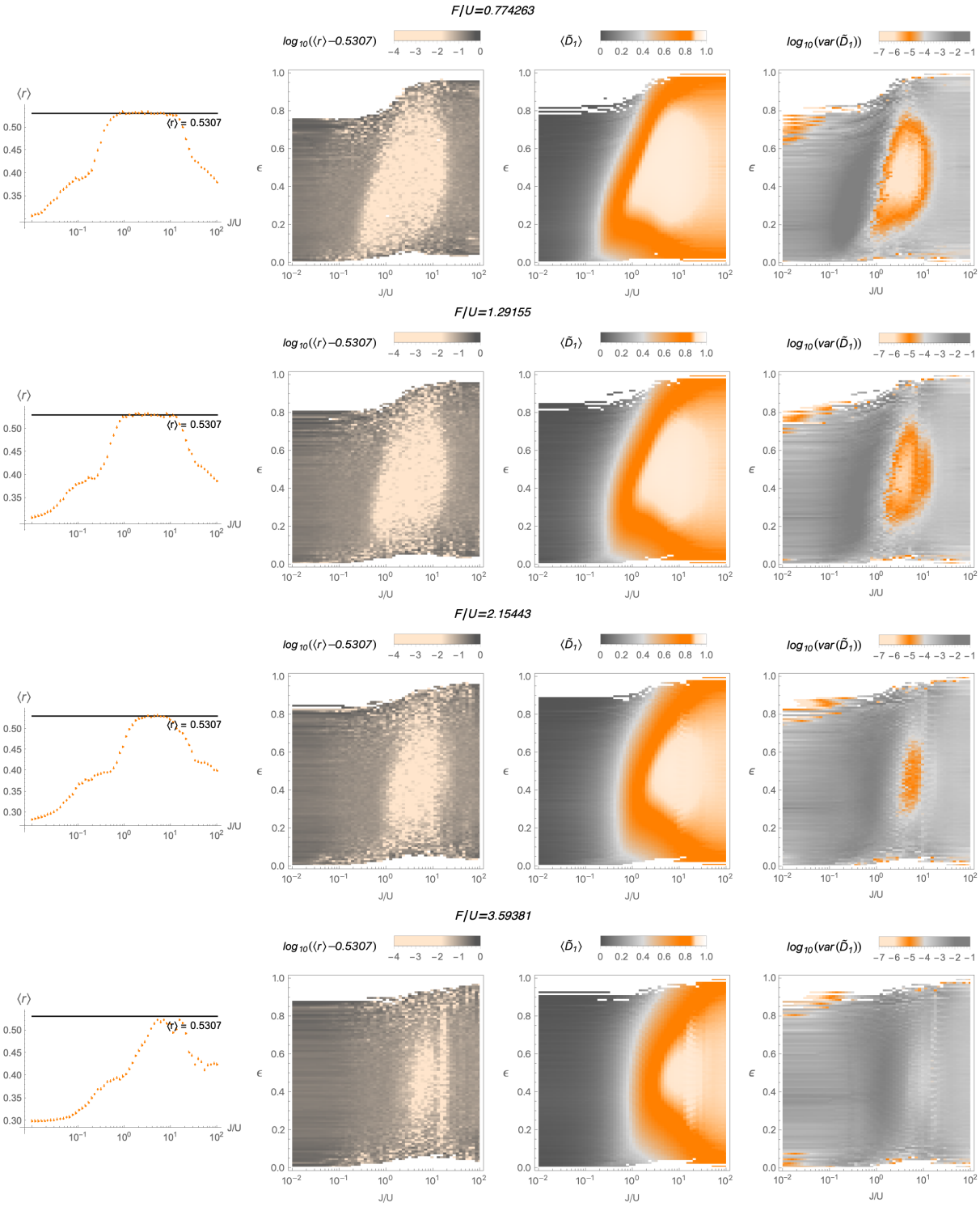

Figure A.1: Spectral and eigenvector properties of the tilted Bose-Hubbard Hamiltonian as functions of J/U for different values of F/U (increasing from top to bottom). The shown figures of merit are (from left to right), energy-averaged $\langle r \rangle$, energy-resolved difference $\langle r \rangle - \langle r_{GOE} \rangle$, mean value of first generalized fractal dimension and variance of first generalized fractal dimension.

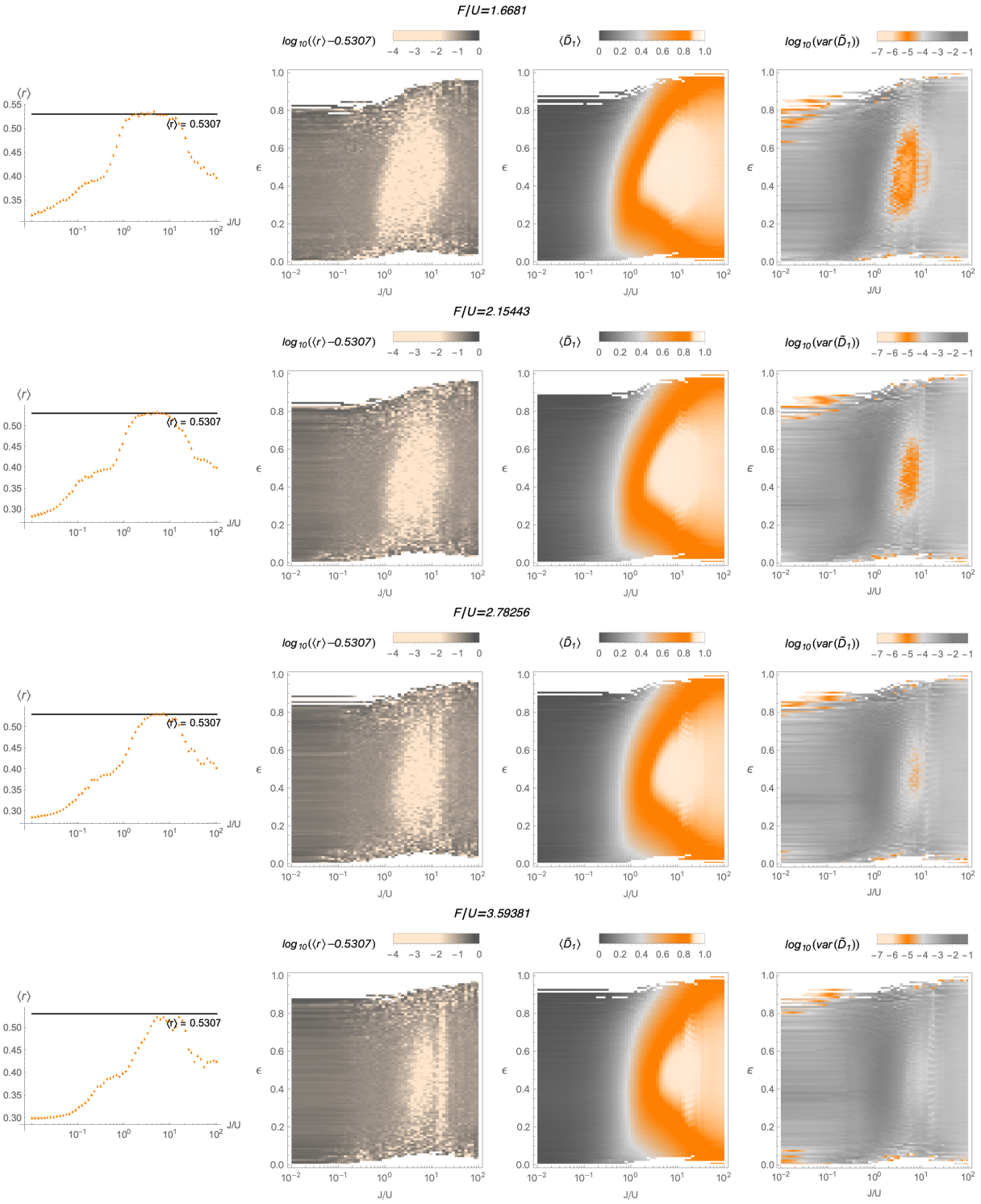

Figure A.1: Spectral and eigenvector properties of the tilted Bose-Hubbard Hamiltonian as functions of J/U for different values of F/U (increasing from top to bottom). The shown figures of merit are (from left to right), energy-averaged $\langle r \rangle$, energy-resolved difference $\langle r \rangle - \langle r_{GOE} \rangle$, mean value of first generalized fractal dimension and variance of first generalized fractal dimension.

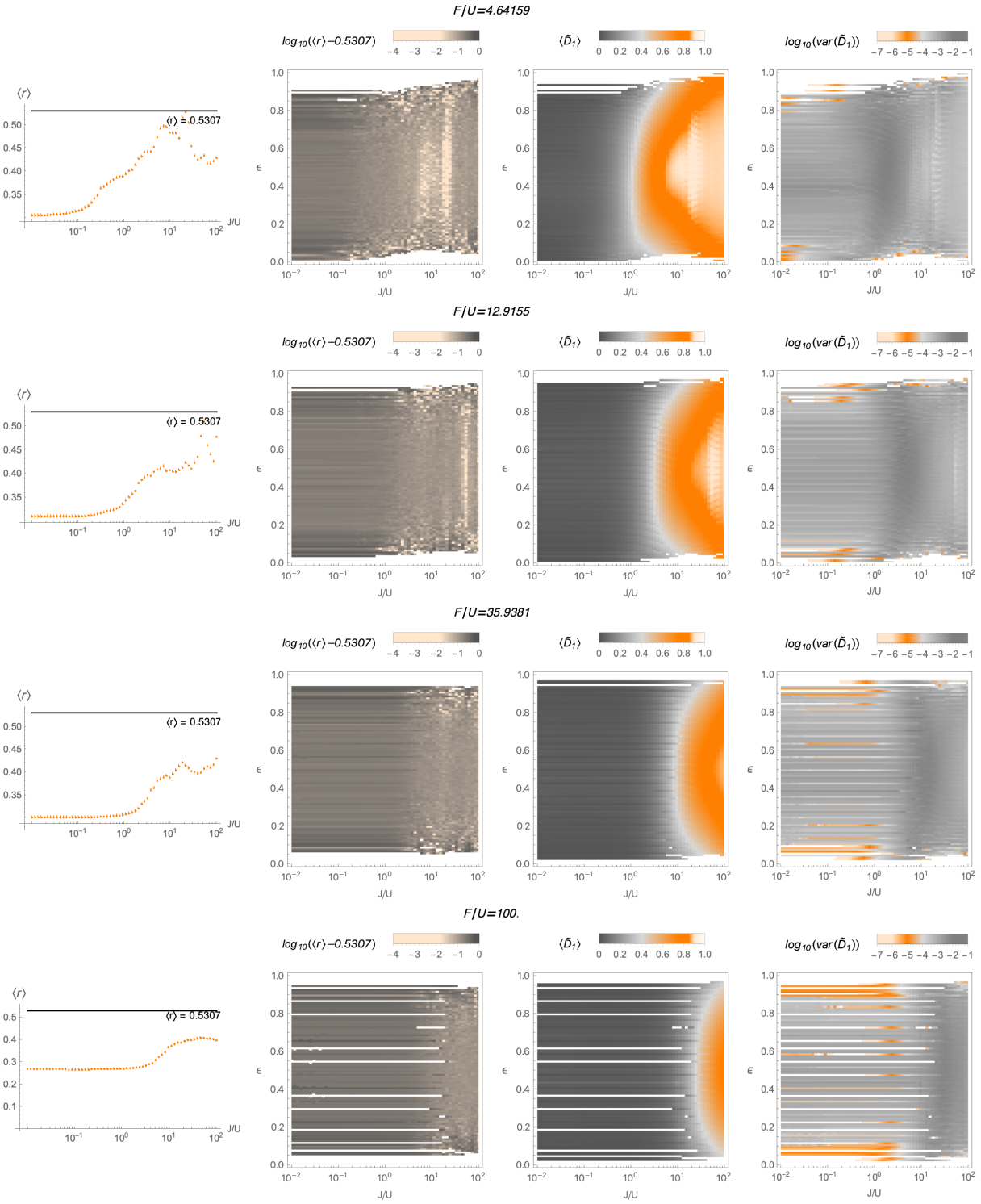

Figure A.1: Spectral and eigenvector properties of the tilted Bose-Hubbard Hamiltonian as functions of J/U for different values of F/U (increasing from top to bottom). The shown figures of merit are (from left to right), energy-averaged $\langle r \rangle$, energy-resolved difference $\langle r \rangle - \langle r_{GOE} \rangle$, mean value of first generalized fractal dimension and variance of first generalized fractal dimension.

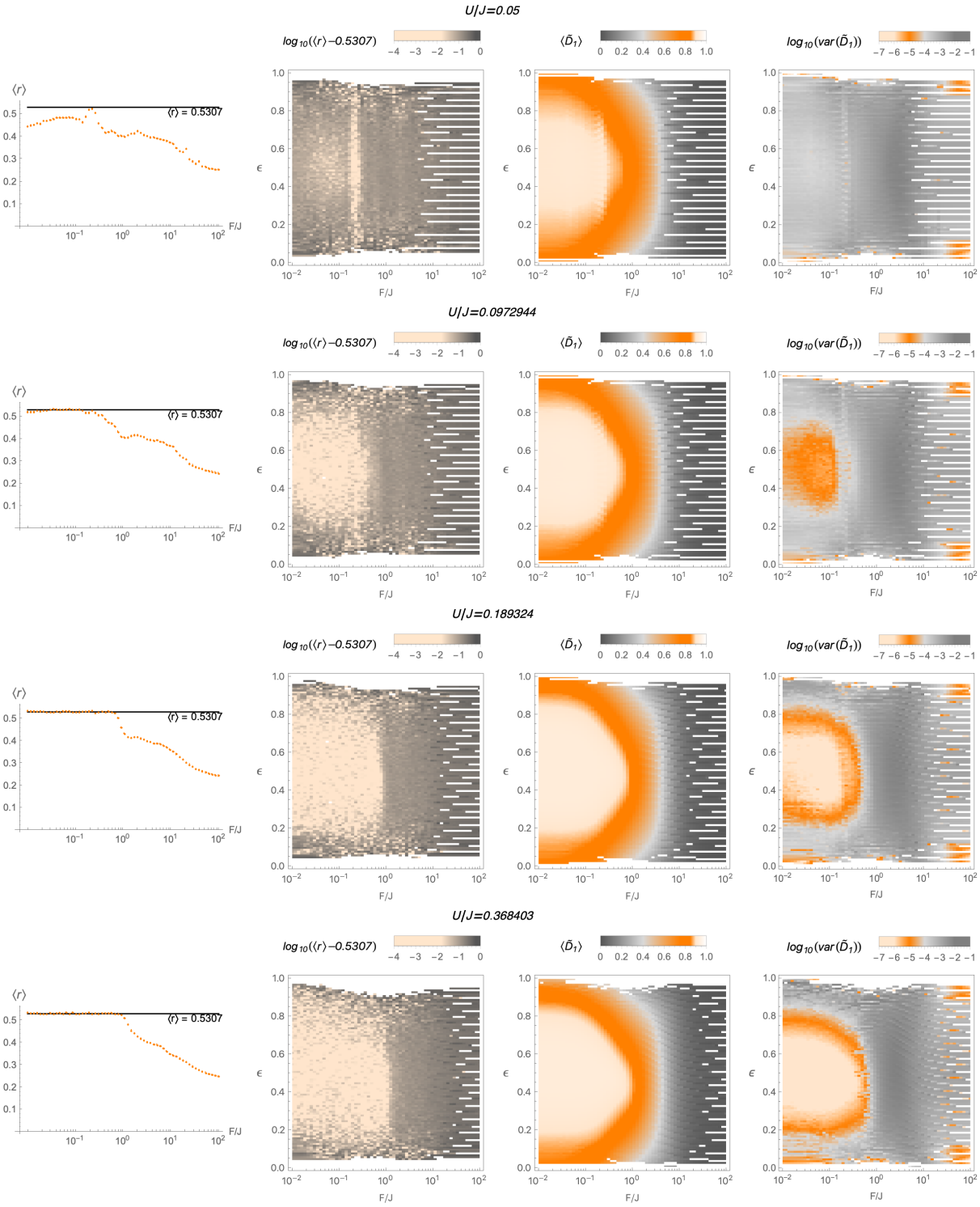

Figure A.2: Spectral and eigenvector properties of the tilted Bose-Hubbard Hamiltonian as functions of F/J for different values of U/J (increasing from top to bottom). The shown figures of merit are (from left to right), energy-averaged $\langle r \rangle$, energy-resolved difference $\langle r \rangle - \langle r_{GOE} \rangle$, mean value of first generalized fractal dimension and variance of first generalized fractal dimension.

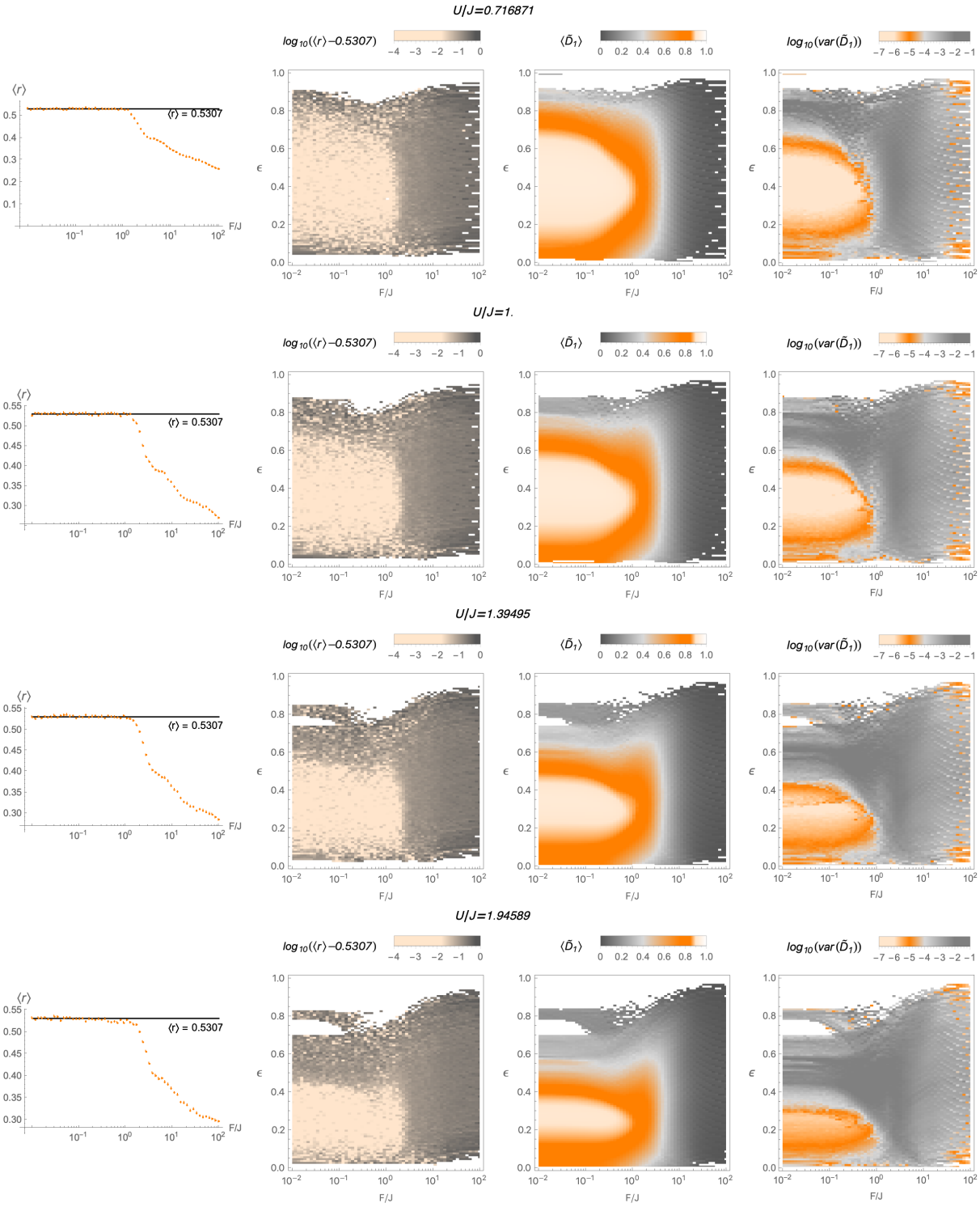

Figure A.2: Spectral and eigenvector properties of the tilted Bose-Hubbard Hamiltonian as functions of F/J for different values of U/J (increasing from top to bottom). The shown figures of merit are (from left to right), energy-averaged $\langle r \rangle$, energy-resolved difference $\langle r \rangle - \langle r_{GOE} \rangle$, mean value of first generalized fractal dimension and variance of first generalized fractal dimension.

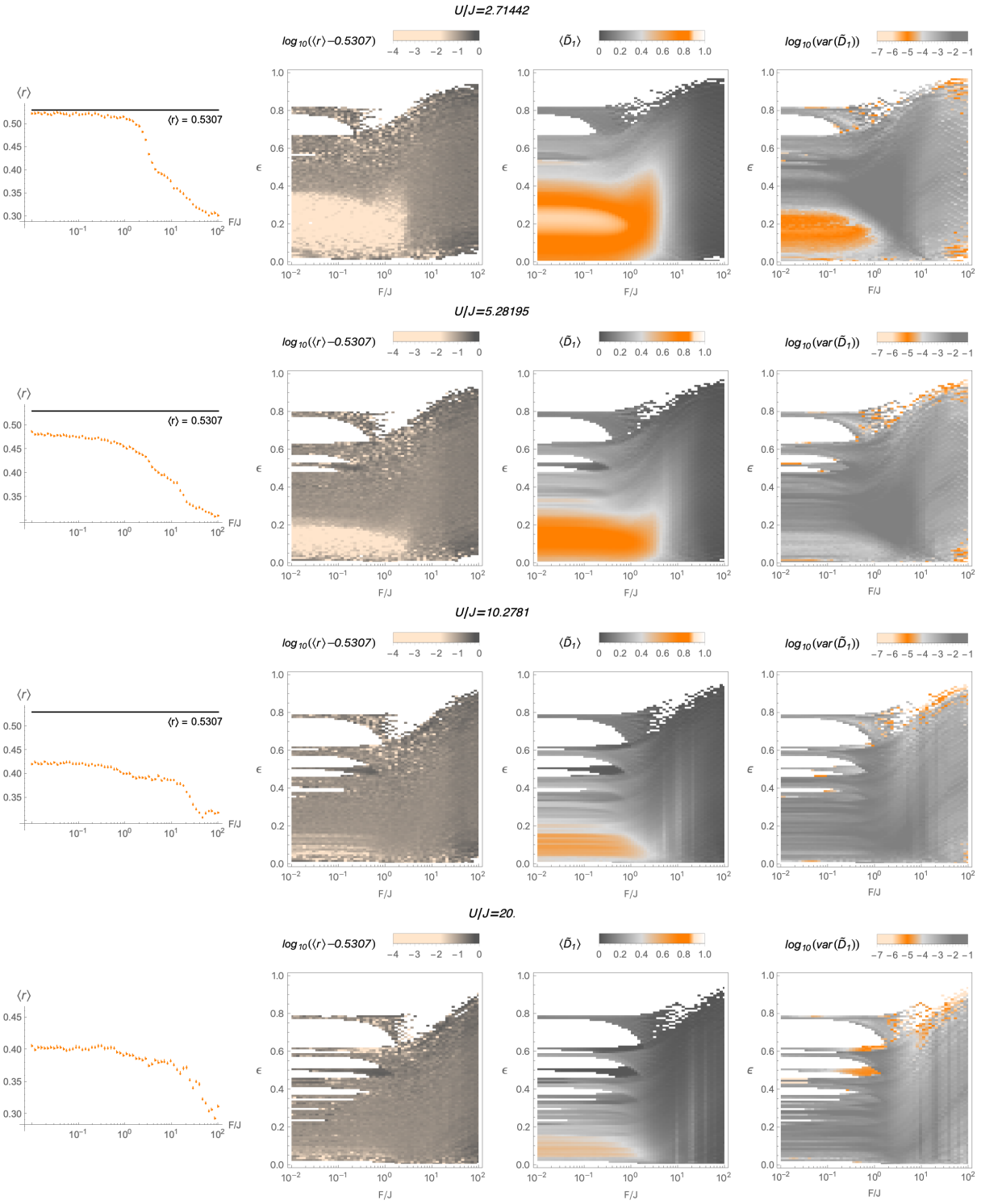

Figure A.2: Spectral and eigenvector properties of the tilted Bose-Hubbard Hamiltonian as functions of F/J for different values of U/J (increasing from top to bottom). The shown figures of merit are (from left to right), energy-averaged $\langle r \rangle$, energy-resolved difference $\langle r \rangle - \langle r_{GOE} \rangle$, mean value of first generalized fractal dimension and variance of first generalized fractal dimension.

B | Calculation of $\langle \hat{H}^2 \rangle$ on the $|1, 1, ..., 1\rangle$ state.

The calculations made to derive the expression shown in Eq. (4.20) are developed in this Appendix. The Hamiltonian shown in Eq. (2.14) can be written as

$$\hat{H} = \hat{h}_{tun} + \hat{h}_{int} + \hat{h}_{tilt}. \tag{B.1}$$

Hence, its square reads

$$\hat{H}^2 = \hat{h}_{tun}^2 + \hat{h}_{tun}(\hat{h}_{int} + \hat{h}_{tilt}) + (\hat{h}_{int} + \hat{h}_{tilt})\hat{h}_{tun} + (\hat{h}_{int} + \hat{h}_{tilt})^2, \tag{B.2}$$

where the only relevant term is the first one, as the other ones will give an expectation value of zero. Hence, let us evaluate $\langle \hat{h}_{tun}^2 \rangle$. First of all, one should write the form of $\hat{h}_{tun}^2$,

$$\hat{h}_{tun}^2 = J^2 \sum_{l=1}^{L-1} (\hat{b}_{l+1}^\dagger \hat{b}_l + \hat{b}_l^\dagger \hat{b}_{l+1}) \sum_{j=1}^{L-1} (\hat{b}_{j+1}^\dagger \hat{b}_j + \hat{b}_j^\dagger \hat{b}_{j+1}) = \tag{B.3}$$

$$= J^2 \sum_{l=1}^{L-1} \sum_{j=1}^{L-1} (b_{l+1}^\dagger b_l b_{j+1}^\dagger b_j + b_{l+1}^\dagger b_l b_j^\dagger b_{j+1} + b_l^\dagger b_{l+1} b_{j+1}^\dagger b_j + b_l^\dagger b_{l+1} b_j^\dagger b_{j+1}). \tag{B.4}$$

Evaluating $\langle 1, 1, ..., 1 | \hat{h}_{tun}^2 | 1, 1, ..., 1 \rangle$ will have non-zero terms only when $l = j$. This can be reasoned by calculating $\hat{h}_{tun}^2 | 1, 1, ..., 1 \rangle$,

$$\hat{h}_{tun}^2 | 1, 1, ..., 1 \rangle = \tag{B.5}$$

$$= J^2 \sum_{l=1}^{L-1} \sum_{j=1}^{L-1} (\underbrace{b_{l+1}^\dagger b_l b_{j+1}^\dagger b_j}_{\text{Term 1}} + \underbrace{b_{l+1}^\dagger b_l b_j^\dagger b_{j+1}}_{\text{Term 2}} + \underbrace{b_l^\dagger b_{l+1} b_{j+1}^\dagger b_j}_{\text{Term 3}} + \underbrace{b_l^\dagger b_{l+1} b_j^\dagger b_{j+1}}_{\text{Term 4}}) | 1, 1, ..., 1 \rangle. \tag{B.6}$$

The action of term 1 on $|1, 1, ..., 1\rangle$ consists in moving one boson from site j to site $j + 1$, and then moving one boson from site l to site $l + 1$. Hence, the action of term 1 over the $|1, 1, ..., 1\rangle$ state will not return the same state but another orthogonal to it. Consequently, it will not contribute to the expectation value.

On the other hand, term 2 moves one boson from site $j + 1$ to site j, and then moves one boson from site l to site $l + 1$. If $j = l$, the action of term 2 on the $|1, 1, ..., 1\rangle$ state will return the same state. Thus, its expectation value will not be zero.

The action of term 3 moves one boson from site j to site $j + 1$, and also moves a boson from site $l + 1$ to site l. Therefore, when $l = j$, the action of term 3 on $|1, 1, ..., 1\rangle$ will give back the same state, hence contributing to the expectation value.

Term 4 acts similarly to term 1, as it removes one boson from site $j+1$ and puts it in site j, as well as it takes one boson from site $l+1$ to site l. There is no possibility that the action of term 4 on $|1,1,...,1\rangle$ returns the same state, so it will give another one orthogonal to it. Hence, its expectation value will be zero.

It can therefore be concluded that the only terms in Eq. (B.5) that are relevant are the second and third ones, and only when $j=l$. Thus, we can calculate the expectation value by only considering such terms,

$$\langle \hat{h}^2_{tun} \rangle = J^2 \langle 1,1,...,1| \sum_{j=1}^{L-1} (b^\dagger_{l+1} b_l b^\dagger_j b_{j+1} + b^\dagger_l b_{l+1} b^\dagger_{j+1} b_j) |1,1,...,1\rangle. \tag{B.7}$$

Using the relations in Eqs. (2.5) and (2.6), one can see that

$$\langle \hat{h}^2_{tun} \rangle = J^2 \langle 1,1,...,1| \sum_{j=1}^{L-1} (b^\dagger_{l+1} b_{l+1} + b^\dagger_{j+1} b^\dagger_j b_j b_{j+1} + b^\dagger_j b_j + b^\dagger_j b^\dagger_{j+1} b_{j+1} b_j) |1,1,...,1\rangle. \tag{B.8}$$

Then, recalling Eq. (2.7),

$$\langle \hat{h}^2_{tun} \rangle = J^2 \langle 1,1,...,1| \sum_{l=1}^{L-1} (\hat{n}_{l+1} + \hat{n}_{l+1}\hat{n}_l + \hat{n}_l + \hat{n}_l \hat{n}_{l+1}) |1,1,...,1\rangle. \tag{B.9}$$

Thus, it can be straightforwardly seen that

$$\langle \hat{h}^2_{tun} \rangle = \langle \hat{H}^2 \rangle = 4J^2(N-1). \tag{B.10}$$